



ISTITUTO NAZIONALE DI RICERCA METROLOGICA Repository Istituzionale

The Boltzmann Project

This is the author's accepted version of the contribution published as:

Original

The Boltzmann Project / Fischer, J.; Fellmuth, B.; Gaiser, C.; Zandt, T.; Pitre, L.; Sparasci, F.; Plimmer, M. D.; de Podesta, M.; Underwood, R.; Sutton, G.; Machin, G.; Gaviolo, R. M.; Madonna Ripa, D.; Steur, P. P. M.; Qu, J.; Feng, X. J.; Zhang, J.; Moldover, M. R.; Benz, S. P.; White, D. R.; Gianfrani, L.; Castrillo, A.; Moretti, L.; Darquié, B.; Moufarej, E.; Daussey, C.; Briaudeau, S.; Kozlova, O.; Risehari, L.; Segovia, J. J.; Martín, M. C.; del Campo, D.. - In: METROLOGIA. - ISSN 0026-1394. - 55:(2018), pp. 1-20.

Availability:

This version is available at: 11696/59965 since: 2021-03-03T15:02:58Z

Publisher:

IOP

Published

DOI:

Terms of use:

This article is made available under terms and conditions as specified in the corresponding bibliographic description in the repository

Publisher copyright

Institute of Physics Publishing Ltd (IOP)

IOP Publishing Ltd is not responsible for any errors or omissions in this version of the manuscript or any version derived from it. The Version of Record is available online at DOI indicated above

(Article begins on next page)



ACCEPTED MANUSCRIPT

The Boltzmann project

To cite this article before publication: Joachim Fischer *et al* 2018 *Metrologia* in press <https://doi.org/10.1088/1681-7575/aaa790>

Manuscript version: Accepted Manuscript

Accepted Manuscript is “the version of the article accepted for publication including all changes made as a result of the peer review process, and which may also include the addition to the article by IOP Publishing of a header, an article ID, a cover sheet and/or an ‘Accepted Manuscript’ watermark, but excluding any other editing, typesetting or other changes made by IOP Publishing and/or its licensors”

This Accepted Manuscript is © 2018 BIPM & IOP Publishing Ltd.

During the embargo period (the 12 month period from the publication of the Version of Record of this article), the Accepted Manuscript is fully protected by copyright and cannot be reused or reposted elsewhere.

As the Version of Record of this article is going to be / has been published on a subscription basis, this Accepted Manuscript is available for reuse under a CC BY-NC-ND 3.0 licence after the 12 month embargo period.

After the embargo period, everyone is permitted to use copy and redistribute this article for non-commercial purposes only, provided that they adhere to all the terms of the licence <https://creativecommons.org/licenses/by-nc-nd/3.0>

Although reasonable endeavours have been taken to obtain all necessary permissions from third parties to include their copyrighted content within this article, their full citation and copyright line may not be present in this Accepted Manuscript version. Before using any content from this article, please refer to the Version of Record on IOPscience once published for full citation and copyright details, as permissions will likely be required. All third party content is fully copyright protected, unless specifically stated otherwise in the figure caption in the Version of Record.

View the [article online](#) for updates and enhancements.

The Boltzmann Project

J Fischer, B Fellmuth, C Gaiser, T Zandt

Physikalisch-Technische Bundesanstalt (PTB), Abbestrasse 2-12, 10587 Berlin, Germany

L Pitre, F Sparasci, M D Plimmer

Laboratoire Commun de Métrologie (LNE-CNAM), 61 rue du Landy, 93210 La Plaine-Saint-Denis, France

M de Podesta, R Underwood, G Sutton, G Machin

National Physical Laboratory (NPL), Hampton Road, Teddington, TW11 0LW, United Kingdom

R M Gavioso, D Madonna Ripa, P P M Steur

Istituto Nazionale di Ricerca Metrologica (INRiM), Strada delle Cacce 91, 10135 Torino, Italy

J Qu, X J Feng, J Zhang

National Institute of Metrology (NIM), Beijing 100029, People's Republic of China

M R Moldover, S P Benz

National Institute of Standards and Technology (NIST), Gaithersburg and Boulder, USA

D R White

Measurement Standards Laboratory of New Zealand (MSL), Lower Hutt, New Zealand

L Gianfrani, A Castrillo, L Moretti

Dipartimento di Matematica e Fisica, Università degli Studi della Campania "Luigi Vanvitelli" Viale Lincoln 5, 81100 Caserta, Italy

B Darquié, E. Moufarej, C Daussy

Université Paris 13, Sorbonne Paris Cité, CNRS, UMR 7538, Laboratoire de Physique des Lasers (LPL), 93430 Villetaneuse, France

S Briau deau, O Kozlova, L Risegari

Laboratoire national de métrologie et d'essais (LNE), 1 rue Gaston Boissier, 75724 Paris, France

J J Segovia, M C Martín

TERMOCAL Research Group, University of Valladolid (UVa), Paseo del Cauce 59, 47011 Valladolid, Spain

D del Campo

Centro Español de Metrología (CEM), Alfar 2, 28760 Tres Cantos, Madrid, Spain

Abstract

The International Committee for Weights and Measures (CIPM), at its meeting in October 2017, followed the recommendation of the Consultative Committee for Units (CCU) on the redefinition of the kilogram, ampere, kelvin and mole. For the redefinition of the kelvin, the Boltzmann constant will be fixed with the numerical value $1.380\,649 \times 10^{-23} \text{ J K}^{-1}$. The relative standard uncertainty to be transferred to the thermodynamic temperature value of the triple point of water will be 3.7×10^{-7} , corresponding to an uncertainty in temperature of 0.10 mK, sufficiently low for all practical purposes. With the redefinition of the kelvin, the broad research activities of the temperature community on the determination of the Boltzmann constant have been very successfully completed. In the following, a review of the determinations of the

1
2
3 Boltzmann constant k , important for the new definition of the kelvin and performed in the last
4 decade, is given.

5
6 **Keywords:** fundamental constant, Boltzmann constant, International System of Units (SI), revised SI,
7 primary thermometry
8
9

10 11 12 **1. Determination of the Boltzmann constant and the new kelvin**

13
14 In 1827, the Scottish botanist Robert Brown observed moving tiny particles suspended in
15 water. All attempts to explain this effect – later called Brownian motion – initially failed. It was
16 only Albert Einstein who realised that the movement of the small particles in the liquid was
17 caused by continual collisions of the water molecules. In 1905, he submitted his work to the
18 "Annalen der Physik" [1], in which he explained the Brownian motion. Einstein's description
19 matched the then very new molecular theory of heat. The warmer the water, for example, the
20 greater the mean velocity by which the water molecules move in an unordered way and thus
21 can cause collisions. Thus, the term "thermodynamics" can be explained: heat is something
22 which is dynamic.
23
24

25
26 It was the French physicist Jean-Baptiste Perrin who confirmed the Brownian motion
27 experimentally with great precision. On the basis of Einstein's model concepts, he was one of
28 the first, in 1908, to experimentally determine the Avogadro constant N_A and thus also the
29 Boltzmann constant k . The fact that the mean of his values showed an error of some 1% for N_A
30 and k can be rated as a quantitative proof for the correctness of the kinetic theory of heat and,
31 thus, also as a further indicator for the atomic structure of matter. In 1926, Perrin was awarded
32 the Nobel Prize for the latter achievement.
33
34
35
36
37
38

39
40 How can the velocity of microscopic particles be used to measure temperature T ? Ludwig
41 Boltzmann derived in the second half of the 19th century the Maxwell-Boltzmann velocity
42 distribution. Therein, the quantity, which is characteristic for the distribution is the microscopic
43 thermal energy kT . By fixing the value of the Boltzmann constant k , the kelvin will be directly
44 linked to the unit of energy – the joule. Boltzmann noticed that in the case of an ideal gas, the
45 thermal energy increases proportionally to the mean kinetic energy of the gas particles. In a
46 closed volume, this energy is directly measurable via the gas pressure and the number of
47 particles. The pressure p is described – with the interaction between the particles being
48 negligible – by means of the equation of state of the ideal gas. The thermometer based on this
49 law is the traditional gas thermometer whose uncertainty, however, is too large for the
50 determination of the Boltzmann constant with the precision required for the redefinition of the
51 kelvin.
52
53
54
55
56
57
58

59 When redefining the kelvin, the measurement uncertainty of the value of the Boltzmann
60 constant k should be comparable to the uncertainty of the realisation used so far. Therefore,

1
2
3 the Consultative Committee for Thermometry (CCT), which was created eighty years ago to
4 advise the International Committee for Weights and Measures (CIPM) on matters of
5 thermometry, recommended to the CIPM that the numerical value of the Boltzmann constant
6 should not be fixed before the following two conditions are met [2]:
7
8

- 9
- 10 • the relative standard uncertainty of the adjusted (mean) value of k is less than 1×10^{-6}
 - 11 • the determination of k is based on at least two fundamentally different methods, of which
12 at least one result for each shall have a relative standard uncertainty less than 3×10^{-6} .
- 13
14

15 These conditions ensure that the best estimate of the triple point of water (TPW) temperature
16 T_{TPW} remains 273.16 K after the redefinition. Measurements taken with only one method are
17 not considered to be sufficiently robust for a fixing of the numerical value. They have to be
18 confirmed by other independent methods to be able to detect and correct hidden errors
19 inherent in the systems.
20
21
22

23 The state of the art of the determinations of the values of physical fundamental constants is
24 periodically reviewed by the CODATA task group on fundamental constants (TGFC). All values
25 of the Boltzmann constant recommended by the TGFC in its adjustments since 1973 are
26 shown in figure 1. The only method used in the experiments contributing to the adjustment of
27 1973 was constant volume gas thermometry (CVGT) [3]. The next adjustment, dated 1986 [4],
28 exhibits a decrease in uncertainty by nearly a factor of four. This was obtained by switching
29 from difficult-to-measure extensive quantities in CVGT to the more accurately measurable
30 intensive quantity speed of sound. This method is called acoustic gas thermometry (AGT) [5].
31 Another factor of five was gained by introducing spherical resonators in AGT [6] replacing the
32 cylindrical systems (c-AGT) used by Colclough and Quinn. We note that all three adjustments
33 from 1998 to 2006 [7, 8, 9] were based only on the same seminal measurement at the National
34 Institute of Standards and Technology (NIST). The final step forward was achieved by the
35 international Boltzmann project [10], whose results contributed essentially to the adjustments of
36 2010, 2014 and 2017 [11, 12, 13].
37
38
39
40
41
42
43
44
45
46
47
48
49
50
51
52
53
54
55
56
57
58
59
60

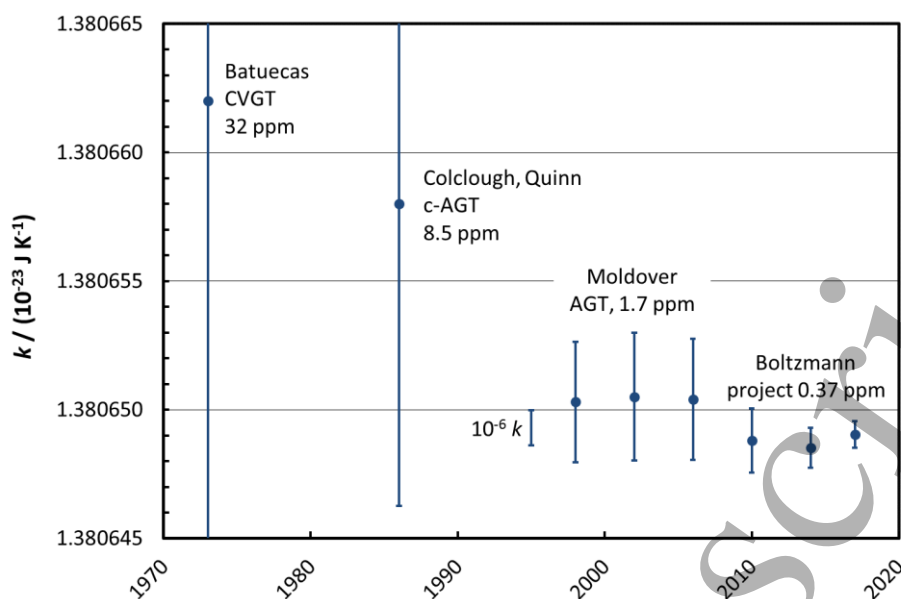


Figure 1. History of the adjusted values of the Boltzmann constant taken from the periodic reviews of the CODATA TGFC with relative uncertainties indicated. Contributing measurements and method indicated. Note that on the time axis are the dates of the CODATA adjustments, not the dates of the contributing measurements. The error bars indicate standard uncertainties.

In the following, this project and its outcomes are described in detail leading to the final relative standard uncertainty of the 2017 adjusted value of the Boltzmann constant of only 3.7×10^{-7} [13].

2. Primary Thermometry

As the microscopic thermal energy kT is not directly accessible by experiment, macroscopic quantities, which are unambiguously correlated with the thermal energy [14], must be measured for the determination of k at a known temperature. The thermometers used for this purpose are called primary thermometers as they do not require any calibration. To attain the smallest possible uncertainties, the experiments were carried out at the triple point of water. As the base unit kelvin is currently defined via this fixed point, this temperature can be realised with the greatest accuracy.

Primary thermometry is performed using a thermometer based on a well-understood physical system, for which the equation of state describing the relation between thermodynamic temperature T and other independent quantities, such as the ideal-gas law or Planck's radiation law, can be written down explicitly without unknown or significantly temperature-dependent constants. Thermodynamic temperature can be obtained by measuring the independent quantities. Accurate thermodynamic temperature values require not only accurate measurements of the independent quantities, but also sufficient understanding of the system to enable a quantitative assessment of departures from the ideal model in order to apply appropriate corrections.

The primary thermometry methods included in this paper fulfil the following criteria, established in the *mise en pratique* of the definition of the kelvin [15]:

- A complete uncertainty budget has been approved by the Consultative Committee for Thermometry (CCT).
- The uncertainty of the realisation of the kelvin is not more than one order of magnitude larger than the state-of-the-art uncertainty achieved with primary thermometry or defined temperature scales, or the uncertainty needed by the stakeholders.
- At least two independent realisations applying the method with the necessary uncertainty exist.
- A comparison of the realisations with the results of already accepted methods has been carried out.
- The methods are applicable over temperature ranges that are acceptable for the stakeholders in metrology, science or industry.
- The experimental technique necessary for applying the methods is documented in sufficient detail in the open literature so that experts in metrology can realise it independently.

In the case of the acoustic gas thermometer, the difficult density determination of the classical gas thermometer is replaced by measuring the speed of sound. Further, the density, which changes with temperature at a constant pressure, can be determined via the dielectric constant or the refractive index. If the conducting electrons of a metallic resistance are used as a "measuring gas", the electrical Johnson noise according to the Nyquist formula is suited for thermometry. Laser spectroscopy provides the kinetic energy of the gas particles from the Doppler broadening of absorption lines.

3. Acoustic gas thermometer

3.1 Introduction

In acoustic gas thermometry (AGT), k is inferred from measurements of the limiting low-pressure value of the squared speed of sound u_0^2 in a monoatomic gas of molar mass M and adiabatic index γ according to [16]:

$$k = \frac{Mu_0^2}{\gamma N_A T} \quad (1)$$

To make measurements with relative standard uncertainties at the level of $u_r \approx 10^{-6}$, all the quantities in Equation 1 must be known with uncertainties at or below $u_r \approx 10^{-6}$. Below, we first look at the features of AGT, that make it especially suitable for low uncertainty measurements, and then we consider the experiments of each member of the Boltzmann collaboration,

1
2
3 highlighting special features or achievements. Finally, we review the combined overall
4 achievements of AGT within the Boltzmann project.

5
6
7 *3.1.1 General features of AGT.* An extensive review of AGT is given in [16]. There are four
8 features of AGT that offer advantages over other techniques of gas thermometry for estimating
9 k . These arise from its theoretical simplicity, the possibility for redundancy and self-checking in
10 resonators, the simultaneous use of microwaves for the *in situ* determination of the dimensions
11 of the resonant cavity and the availability of accurate, theoretical values of gas properties. We
12 discuss each of these in turn below.

13
14
15
16
17 *3.1.2 Theoretical simplicity.* Perhaps the most significant feature of AGT is that there is a simple
18 theoretical link between the speed of sound, u_0 , in a gas and the root mean square molecular
19 speed, v_{RMS} . In the limit of low density for monatomic gases $v_{\text{RMS}} = \sqrt{9/5} u_0$. This simple
20 relationship leads to two experimental advantages over other techniques of gas thermometry.
21 The first is that there is no first-order dependence of the speed of sound on pressure. This
22 arises because in the formula for the speed of sound $u = \sqrt{B/\rho}$ both the bulk modulus B and
23 the mass density ρ depend linearly on pressure. Thus, there is no requirement to make a
24 pressure measurement with similar fractional uncertainty to the target uncertainty in k . The
25 second advantage is that as an intensive measurement, there is no requirement to assess the
26 amount of gas adsorbed on the walls of a container, a significant disadvantage of constant
27 volume gas thermometry.

28
29
30
31
32
33
34
35 *3.1.3 Redundancy in resonators.* A second category of experimental advantages involves the
36 use of resonators to determine the speed of sound. In resonators of any shape, the frequencies
37 of acoustic resonances are linearly related to the speed of sound in the medium, except for a
38 number of relatively small correction terms, the most significant of which arises from the
39 boundary layer near the walls of the resonator. Typically these corrections cannot be measured
40 directly but must be calculated from first principles and the magnitude of the corrections will vary
41 between resonances and resonators.

42
43
44
45
46
47 Any single acoustic resonance could be used to determine u , and the use of multiple modes to
48 estimate u might appear to be simply generating redundant data. However, this redundancy of
49 estimates of u inferred from multiple acoustic resonances is a powerful self-checking feature. If
50 the magnitude of the first-principles corrections were misestimated, then estimates of u derived
51 from different acoustic resonances would be expected to disagree. So the level of agreement
52 amongst estimates of u derived from different acoustic resonances provides a robust
53 assessment of the effectiveness of the corrections for a wide range of perturbations.

54
55
56
57
58 *3.1.4 Combined microwave and acoustic resonators.* The third category of experimental
59 advantage – used by five of the six AGT groups – is the simultaneous use of microwave
60

1
2
3 resonances within the acoustic resonator. In effect, the resonator acts as temporary artefact that
4 facilitates accurate determinations of the ratio $u/c = (\text{speed of sound})/(\text{speed of light})$ from
5 measurements of ratios of acoustic resonance frequencies to microwave resonance
6 frequencies. In this way, the speed of sound is accurately traced to the fundamental constant c
7 without making complex, accurate dimensional measurements [17].
8
9

10
11 The combined microwave and acoustic resonator technique has been developed exquisitely in
12 so-called quasi-spherical resonators in which the resonator is made deliberately slightly
13 aspherical [18]. This shape perturbation is engineered to split the triply-degenerate TM_{1n} and
14 TE_{1n} resonances into three singlet resonances each of which reflects the average radius in one
15 of three orthogonal directions. If the perturbation, which creates this splitting, is a smooth well-
16 characterized distortion such as that arising in a triaxial ellipsoid, the correction to acoustic and
17 microwave eigenvalues can be calculated to second-order or higher [19, 20, 21]. This has
18 allowed *in situ* measurement of the resonator's dimensions with uncertainties on the order of 2
19 parts in 10^7 [22].
20
21

22
23 *3.1.5 Theoretical values of the thermophysical properties.* Progress in AGT stimulated
24 calculations of the properties of gaseous helium from the basic principles of quantum mechanics
25 and statistical mechanics. At low densities, the calculated values of the thermal conductivity and
26 the real-gas corrections to the speed of sound are more accurate than the measured values.
27 Therefore, the calculated values are used to correct the acoustic frequencies and to constrain or
28 eliminate the extrapolation to zero pressure. For AGT using argon, values of the thermal
29 conductivity traceable to theory are used in a similar way [23]. For dielectric-constant gas
30 thermometry (DCGT), theory-based property values [24] have been very good indicators for the
31 quality of data, but due to the extrapolation to zero pressure, the real-gas properties are not
32 needed. (If constant-volume gas thermometry were conducted today, it too would benefit from
33 theory-based virial coefficients for the real gas.)
34
35
36
37
38
39
40
41
42
43

44 *3.2 Differences in implementations*

45
46 Despite the use of a shared technique, the implementations of AGT for the determination of k
47 have been significantly different (table 1). Thus, collectively, many of the possible unanticipated
48 systematic biases have been shown to have been correctly accounted for.
49
50
51
52
53
54
55
56
57
58
59
60

Table 1. Institutions involved in determining k using AGT (see authors list for team abbreviations). Details of the resonators and gases used for the final determinations of k are listed. We omit earlier estimates from each institution.

Team	Shape	Size	Material	Gas	Reference
NIST	Sphere	3 litres, radius 89 mm	Steel	Ar	[6]
INRiM	Misaligned hemispheres	3 litres, radius 89 mm	Copper	He	[25]
LNE-CNAM	Triaxial Ellipsoid	3 litres, radius 89 mm	Copper	He	[26]
NIM	Cylinders	Length 80 mm radius 80 mm	Steel and Copper	Ar	[27]
NPL	Triaxial Ellipsoid	1 litre, radius 63 mm	Copper	Ar	[28]
UVa/CEM	Triaxial Ellipsoid	0.25 litre, radius 40 mm	Gold-Coated Steel	Ar	[29]

3.2.1 NIST. Although not part of the project [10], we mention the NIST measurement of k [6] of 1988 because of the seminal nature of the work. They estimated k using argon gas in a spherical 3-litre stainless steel resonator the volume of which was estimated by mercury pycnometry. The switch to using spherical rather than cylindrical resonators required substantial development of the theory describing the operation of such resonators in real world situations, most specifically, the interaction of the acoustic modes with the mechanical ‘shell’ vibrations [30], and the effect of small perturbations to the main acoustic resonances [31, 32]. These works formed the foundation on which AGT in the Boltzmann collaboration was built.

3.2.2 INRiM. The INRiM measurement of 2015 [25] was carried out using helium gas in a three litre, diamond turned spherical copper resonator in which the hemispheres had been marginally misaligned. This misalignment has been shown to create an effective ellipsoid to allow the estimation of the volume of the resonator by microwaves. The high electrical conductivity of the copper meant that a displacement of the hemispheres by only 15 micrometres was sufficient to allow good microwave measurements while producing only a very small additional acoustic perturbation.

The use of helium has advantages and disadvantages. The most significant advantage is that the thermophysical and electromagnetic properties of helium can be calculated with an uncertainty much lower than the uncertainty, with which the properties of any other gas can be calculated or measured. However, the most critical disadvantage is that the speed of sound in helium is more sensitive to the presence of other gas species, chemical or isotopic. A key improvement of this work involved an assessment of isotopic contamination by ^3He , and a cross-check of the estimate of helium impurities was made by using the mass spectrometry facilities at PTB. Finally, an overall relative standard uncertainty of $u_r = 1.06 \times 10^{-6}$ was achieved.

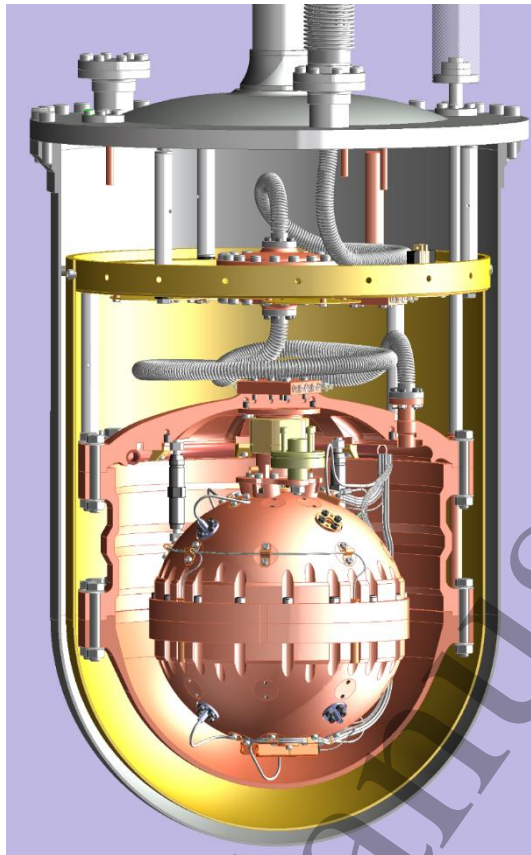


Figure 2. The LNE-CNAM resonator BCU4 used for the lowest uncertainty estimate of the Boltzmann constant. The copper resonator is assembled from two diamond-turned hemispheres to create a triaxial ellipsoid with an internal volume of approximately 3 litre.

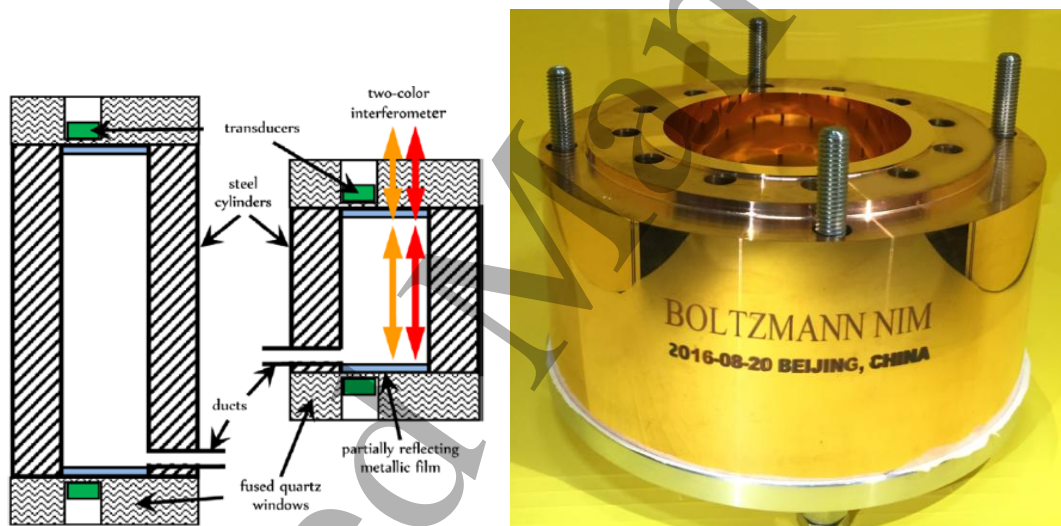
3.2.3 LNE-CNAM. The LNE-CNAM measurement of 2017 [26] was carried out using helium gas in a three litre, diamond-turned quasi-spherical resonator (figure 2) and has the lowest uncertainty in the determination of k . It thus represents the culmination of three decades of work that sprang from the original NIST 1988 measurement [6]. The low uncertainty was achieved by exceptional implementation of these decades of research, coupled with techniques for establishing the purity of the helium with unprecedentedly low uncertainty.

The isotopic purity was established by collaborative mass-spectrometer studies, and the chemical purity was established *in situ* using a double helium cold trap experiment. These two steps allowed the full realisation of the potential for uncertainty reduction resulting from the ability to perform *ab initio* calculations of the thermophysical properties of helium. Overall the final result had a relative standard uncertainty of 0.60×10^{-6} , and significantly the result was in good agreement with the previous estimates made using argon [33] and helium [34, 35] in a 0.5 litre quasi-sphere. Combining all results yielded a further reduction in the institutional uncertainty estimate of k to $u_r = 0.56 \times 10^{-6}$ [26].

3.2.4 NIM. The NIM result of 2017 [27] was based on measurements using argon gas in a series of cylindrical resonators 80 mm in diameter, made either entirely from copper [27], or from steel cylinders with quartz endplates [36-38]. The spectrum of acoustic resonances in

1
2
3 cylinders is distinctly different from that in spheres and quasi-spheres, and the dissipation of
4 acoustic energy also has a quite distinct character. Together these features make acoustic
5 measurements in cylinders more challenging than those in spheres. However, they also test the
6 underlying theory for possible systematic effects more thoroughly.
7
8

9
10 Another significant difference in the NIM measurements compared to the project [10]
11 participants was the use of transparent quartz endplates which allowed determination of the
12 length of the cavity by two colour optical interferometry (figure 3) [36]. Additionally, the NIM
13 team used piezoelectric transducers to couple sound into and out of the resonators [38]. The
14 complex end-plate design led to a novel scheme, which evaluated the perturbations caused
15 by the end plates by using pairs of cylinders, which differ in length by a factor two. In such
16 cylinder pairs, major perturbations caused by the quartz end plates can be more clearly
17 identified. In practice an undesired resonant coupling between the two cavities or the
18 pressure vessel limited the performance of the experiment [39] and the relative standard
19 uncertainties achieved were 7.86×10^{-6} , 3.35×10^{-6} , 3.82×10^{-6} and 3.36×10^{-6} , respectively.
20
21
22
23
24
25
26
27
28



43
44 **Figure 3.** NIM have developed several cylindrical resonators. (left): Schematic illustration of the use
45 of two cylinders differing in length by a factor two, in which the end effects can be cancelled out.
46 (right): A diamond-turned copper cylinder using the final NIM experiments.

47
48 In their final measurements, NIM used a single-cylinder made of diamond-turned copper with
49 copper end plates [27], which yielded an estimate of k with an uncertainty of 4.22×10^{-6} . The NIM
50 team then established a weighted mean of all their determinations with a relative standard
51 uncertainty of 2.0×10^{-6} considering carefully the correlations of various components of
52 uncertainty.
53
54

55
56 **3.2.5 NPL-Cranfield.** The NPL measurement of k in 2013 [28] was made using argon gas in the
57 NPL-Cranfield resonator, a one litre, diamond-turned quasi-spherical resonator. The exceptional
58 shape-fidelity of the resonator led to exceptionally close agreement between the value of k
59 inferred from different acoustic modes, and exceptional agreement between the radius inferred
60

1
2
3 from different microwave modes. This agreement was checked for systematic errors by auxiliary
4 studies involving co-ordinate measuring machines [40] and pycnometry of diamond-turned
5 quasi-spherical resonators with water [41]. Additionally, the degree of acoustic perfection led to
6 the discovery of a line-narrowing effect in the resonances [42] that had been independently
7 discovered by the INRiM group [112]. The novel data analysis [28, 43] allowed the identification
8 of anomalous modes that might have subtly affected the inference of k .
9
10
11

12
13 However, the initial published value was later shown to contain an erroneous estimate of the
14 molar mass of argon. This was identified in a multi-institution study of argon samples involving
15 acoustic measurements at LNE-CNAM, and mass spectroscopic measurements at the Korea
16 Research Institute of Standards and Science (KRISS) [44]. This led first to a correction with an
17 enlarged uncertainty [45] and, finally, to a study which identified the source of the error as
18 contamination of the argon gas by atmospheric air. In 2017 a final revised estimate with a
19 relative standard uncertainty of 0.70×10^{-6} was published [46].
20
21
22
23

24
25 *3.2.6 CEM and University of Valladolid.* The 2017 measurement by Universidad de Valladolid
26 (UVa) in collaboration with CEM used argon gas in a gold-coated stainless steel, quasi-
27 spherical resonator with a radius of 40 mm [29]. Several features of the measurement were
28 unique within the project [10]. In particular, the use of a sealed resonator which was fully
29 pressurized during measurements, and novel solid-dielectric capacitance transducers. Initial
30 measurements in an uncoated misaligned resonator led to a larger measurement uncertainty of
31 20×10^{-6} [47] due to the high resistivity of stainless steel and the simple shape of the resonator.
32 But using a quasi-spherical gold-coated resonator, the same measurement system could
33 achieve a relative standard uncertainty of 6.7×10^{-6} [29].
34
35
36
37
38
39

40 *3.3 Overall results*

41
42 Table 2 shows the final measurement uncertainty achieved by the different groups categorized
43 by the different limiting uncertainties. By averaging different measurements and taking account
44 of the components of the measurements which are correlated, it is possible to reduce the
45 uncertainty further, but the table shows only the best uncertainty in a single measurement. Let
46 us consider each component of uncertainty in turn.
47
48
49
50
51
52
53
54
55
56
57
58
59
60

Table 2. The lowest uncertainty AGT results from each institution in the Boltzmann collaboration showing the numerical value k and uncertainty contributions arising from key components of the uncertainty budget. The uncertainties are relative standard uncertainty components expressed as parts in 10^6 .

Team [Reference]	k / (10^{-23} J K ⁻¹)	Dimensional	Acoustics	Molar Mass	Temperature	Overall
NIST [6]	1.380 650 2	0.80	0.92	0.81	0.89	1.8
INRiM [25]	1.380 650 9	0.52	0.90	0.37	0.42	1.06
LNE-CNAM [26]	1.380 648 80	0.20	0.40	0.09	0.39	0.60
NIM (Best) [27]	1.380 648 4	1.32	2.93	0.77	0.49	3.35
NPL [46]	1.380 648 62	0.38	0.18	0.39	0.36	0.70
UVa/CEM [29]	1.380 646 7	4.7	4.4	1.5	0.9	6.7

For temperature, it appears that the limiting uncertainty in the realisation of the triple point of water has an estimated standard uncertainty of approximately $u_r \approx 0.4 \times 10^{-6}$. Given that the combined standard uncertainty of the adjusted value of k is $u_r = 0.37 \times 10^{-6}$, we can be assured that the redefinition of the kelvin will add no significant uncertainty to any practical temperature measurement, even those made close to the temperature of the triple point of water.

Regarding the molar mass of the gas, it appears that for argon, the limiting uncertainty is approximately $u_r \approx 0.4 \times 10^{-6}$. This limit arises from the requirement to reference the gravimetric isotope mixtures made by Lee *et al.*, see ref. [44]. However, the outstanding achievement of the project was the uncertainty of $u_r \approx 0.09 \times 10^{-6}$ achieved by Pitre *et al.* [26] in the determination of the helium molar mass by the use of precision mass spectrometry and the implementation of verifiable cold-trap techniques.

Regarding measurements of the dimensions of the resonator, the microwave spectroscopy technique seems to be superior to the two-colour interferometry approach only usable for cylindrical resonators. In general, the lowest uncertainty achieved was $u_r \approx 0.2 \times 10^{-6}$ by the team at LNE-CNAM [26].

Overall, the techniques developed in the project have advanced the state of the art considerably, and each group has extended the operating envelope of acoustic thermometry in a different way. In the near future, many of the techniques and facilities developed will be likely be applied to other fundamental measurements in the fields of gas purity, humidity, thermodynamic temperature and dimensional measurements.

4. Dielectric-constant gas thermometer

4.1 The Experiment

The basic idea of DCGT is to replace the density in the state equation of a gas by the dielectric constant and to measure it by the capacitance changes of a capacitor filled with the gas (see figure 4). If the gas particles do not interact (ideal gas), the working equation can be simply derived by combining the classical ideal-gas law and the Clausius-Mossotti equation [48]. The determination of the Boltzmann constant k by DCGT is based on measuring the pressure dependence of the capacitance of the capacitor, containing the measuring gas helium, at a constant known thermodynamic temperature T , i.e. on measuring isotherms. To achieve the smallest uncertainty, the measurements have to be performed at the TPW, the temperature of which is known by definition. The data pairs of pressure and relative capacitance change are fitted by applying a virial expansion, which considers the interaction of the atoms of the real helium gas and includes thermodynamic temperature as one of the parameters. In particular, the fitting coefficient of the first, linear term, which describes the ideal-gas behaviour, is given by $A_1 = (A_\epsilon/RT + \kappa_{\text{eff}}/3)^{-1}$, where A_ϵ is the molar polarizability and R is the molar gas constant. κ_{eff} denotes the effective compressibility of the capacitor, which describes the change of the capacitance only due to the mechanical deformation caused by the measuring gas. T is the temperature of the TPW, and κ_{eff} is calculated from the materials parameters of the capacitor. Then, the ratio A_ϵ/R of two molar quantities is deduced from A_1 to determine k applying the relation

$$k = \frac{\alpha_0}{3\epsilon_0} \bigg/ \frac{A_\epsilon}{R}, \quad (2)$$

where ϵ_0 is the fixed electrical constant. The atomic dipole polarizability $\alpha_0 = 2.281\,513\,31(23) \times 10^{-41} \text{ C m}^2/\text{V}$ in SI units is calculated *ab initio* with a relative standard uncertainty of 0.1 parts per million (0.1 ppm) [49], where A_ϵ is defined as $A_\epsilon = N_A \alpha_0 / (3\epsilon_0)$, with N_A being the Avogadro constant.

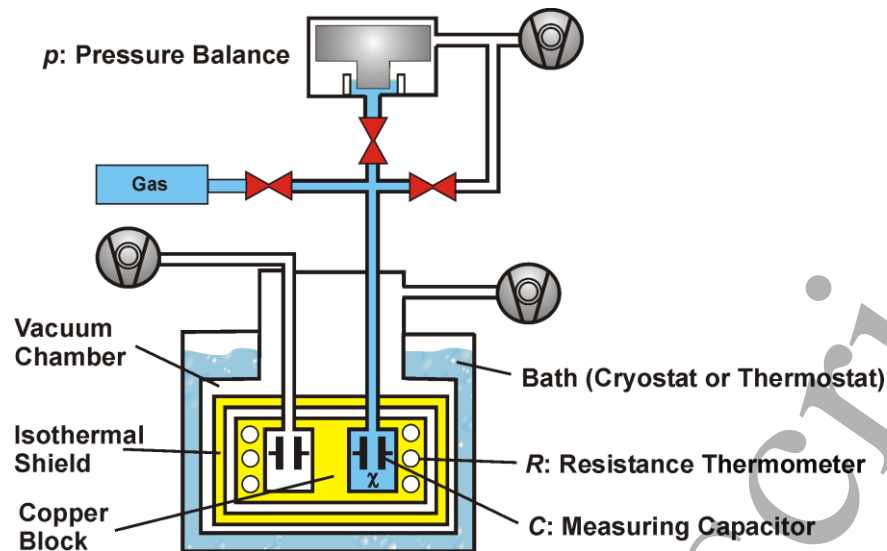


Figure 4. Schematic sketch of the DCGT setup used at PTB (reference capacitor on the left, measuring capacitor on the right). Three quantities must be measured: pressure p , capacitance $C(p)$ and temperature T via the resistance R of a thermometer, which was calibrated at the TPW. $\chi = \epsilon_r - 1$ is the dielectric susceptibility of the gas.

The measurement of the Boltzmann constant by DCGT requires the determination the temperature of the gas, and thus of the capacitor electrodes, traceably to the temperature of the TPW with a standard uncertainty of order 0.1 mK. To obtain a thermal environment of sufficient quality, a three-level arrangement has been realised in the DCGT experimental setup of PTB. Each capacitor is surrounded by a rigid, metallic pressure vessel, which is thermally anchored to the 30 mm thick central copper plate of the measuring system. The temperature of the plate is measured with the aid of three capsule-type standard platinum resistance thermometers, which have been calibrated at the triple points of mercury and water as well as at the melting point of gallium. Besides the central plate, which is located at the bottom and acts as heat sink, the system consists of a top plate, four thick rods connecting the two plates and an isothermal shield, all made from copper. The capacitors in the pressure vessels are, therefore, completely surrounded by an isothermal copper shell. In turn, the measuring system is placed within a vacuum chamber for thermal isolation. Finally, the chamber is inserted in a huge liquid-bath thermostat. The thermal conditions within the experimental setup have been investigated in detail as described in previous papers [50, 51]. A photograph and a detailed design drawing of the measuring system are given in [50].

The liquid-bath thermostat has an overall volume of the liquid of about 800 litres and a central working volume, in which the vacuum chamber is located, with a diameter of 500 mm and a height of 650 mm. The temperature stability and the temperature field at the boundary of the working volume without and with the chamber have been investigated carefully under different experimental conditions. It could be verified that, under optimum conditions, both the

1
2
3 instability and the inhomogeneity of the temperature in the working volume are well below
4 1 mK, as is necessary [51].
5

6 7 4.2 The Capacitors 8

9 The design of the cylindrical measuring capacitor and the material was critical. The use of
10 tungsten carbide (TC) as material for the electrodes and the bed-plate, on which the
11 electrodes are mounted, led to the final design described in detail in [52]. TC has a
12 compressibility that is about a factor of two smaller than that of stainless steel, which was
13 used previously [53]. This led to a reduction of the uncertainty component caused by the
14 effective compressibility κ_{eff} , describing both the change of the capacitance due to the
15 deformation and the relative displacement of the capacitor electrodes under pressure p . In
16 principle, it is also influenced by the change of stray capacitances caused by the deformation
17 of all pieces within the pressure vessel and the vessel itself, but this influence is negligible for
18 the capacitor design discussed in [52].
19

20 The capacitance of an ideal cylindrical capacitor is given by $C_{\text{cyl}} = 2\pi\epsilon l / \ln(d_o/d_i)$ with ϵ being
21 the dielectric constant, l the electrode length, d_o the inner diameter of the outer electrode,
22 and d_i the outer diameter of the inner electrode. Thus, only the relative change $\Delta l/l(p=0)$
23 of l is relevant for the capacitance change under pressure, i.e., κ_{eff} is about one third of the
24 volume compressibility κ_{vol} of the electrode material, which is the inverse of the bulk modulus.
25 This elastic property can be determined with resonant ultrasound spectroscopy (RUS) [54,
26 55], which uses normal-mode resonance frequencies of free vibration as well as data on the
27 shape and the mass of the sample. But it has to be considered that the compressibility
28 measured by RUS is the adiabatic one, whereas for the DCGT the isothermal compressibility
29 is needed. For the conversion from the adiabatic value κ_{ad} to the isothermal one κ_{iso} ,
30 Grüneisen has derived the relation $\kappa_{\text{iso}} = \kappa_{\text{ad}} + TV_m\alpha_V^2/C_p$ [56], with the molar volume V_m , the
31 thermal-expansion coefficient α_V and the molar specific heat capacity C_p at constant
32 pressure.
33

34 Besides deformation and relative displacement, the effective compressibility may also be
35 influenced by the eccentricity and the tilt of the capacitor electrodes. Furthermore, in reality a
36 rigid capacitor is a complicated geometrical object because electrically isolating pieces and
37 stabilizing screws are necessary. Thus, the isothermal compressibility of a composite has to
38 be determined. Using tungsten carbide electrodes and sapphire isolating discs for the
39 construction design described in [52], relative standard uncertainties of κ_{eff} ranging from
40 0.05% to 0.17% were achieved at the TPW. This was possible by checking the mounting of
41 the electrodes applying a coordinate measuring machine and performing simulations with the
42
43
44
45
46
47
48
49
50
51
52
53
54
55
56
57
58
59
60

1
2
3 finite-element method regarding the influences of the relative displacement of the electrodes
4 and stray capacitances (for details see [52]).
5
6

7 Considering the extreme demands concerning the measurement of capacitance changes, a
8 high-resolution and high-precision autotransformer ratio capacitance bridge has been built
9 and tested. Its main component is a home-made high-precision inductive voltage divider
10 used in an autotransformer configuration. For balancing the bridge, adjustable in-phase and
11 quadrature currents can be injected. A detailed uncertainty budget for measuring small
12 capacitance changes is presented in [57]. Considering correlations between main terms in
13 the mathematical model, it has been shown that it is possible to measure capacitance
14 changes of at most a few 0.1% with a relative standard uncertainty below one part per
15 million, i.e., with a standard uncertainty relative to the capacitance value of order one part
16 per billion. The performed consideration of correlations requires that the measuring circuit is
17 fully symmetric. For this reason, the reference capacitor is also located in the measuring
18 system within the vacuum chamber.
19
20
21
22
23
24
25

26 27 *4.3 Results*

28
29 The determination of the Boltzmann constant at the TPW using helium places extreme
30 requirements on the purity of the measuring gas. To prevent contamination of the helium of
31 nominal purity of 99.99999% during handling, a gas purifier (adsorber) and a helium purifier
32 (getter) have been incorporated in the ultra-high-purity gas-handling system. After each
33 measurement of an isotherm, which lasted usually one week, the measuring gas was
34 analysed with the aid of a mass spectrometer to check for a possible contamination
35 especially due to outgassing from the different pieces inside the pressure vessel. This led to
36 an upper limit for the influence of impurities on the result for k . The maximum relative change
37 of the result cannot be more than 1 ppm.
38
39
40
41
42
43

44 To achieve sufficiently detectable capacitance changes by the measuring gas helium,
45 pressures up to 7 MPa had to be measured with a relative standard uncertainty of order
46 1 ppm. This goal was a further challenge because it required characterisation of pressure
47 balances with unprecedented accuracy, and even to improve the national standard of PTB
48 significantly. For absolute pressure measurements in helium up to 7 MPa, a system of
49 special pressure balances was designed, constructed and evaluated. The system includes
50 two pressure-balance platforms, three piston-cylinder units (PCUs) with effective areas of
51 20 cm², and three PCUs of 2 cm². Traceability to the SI base units up to 7 MPa was realised
52 in two steps. First, the zero pressure effective areas of the 20 cm² PCUs have been
53 determined from dimensional measurements. Second, the 2 cm² PCUs have been calibrated
54 against the 20 cm² PCUs by comprehensive cross-float comparisons [58].
55
56
57
58
59
60

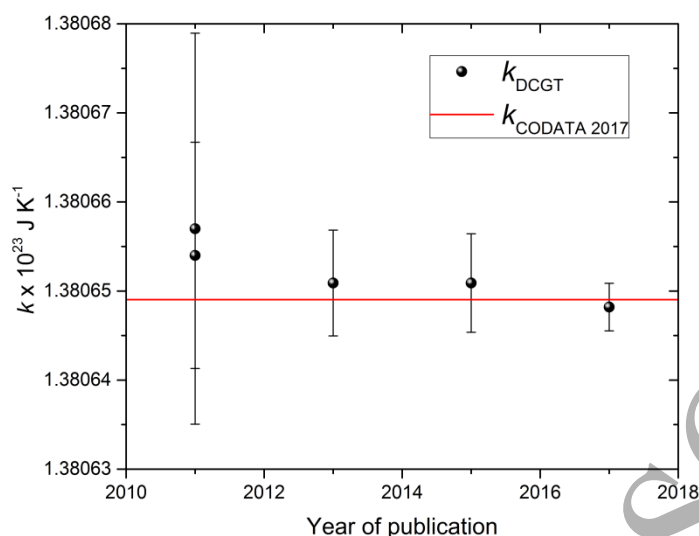


Figure 5. The black dots show the development of the determinations of k with DCGT since 2011. The data is taken from the papers published in 2011 [54, 59], 2013 [60], 2015 [48] and 2017 [52]. The red line shows the CODATA 2017 [13] estimate for k (for more details see text).

In 2013, a second, improved value of the Boltzmann constant k determined by DCGT at the TPW ($k = 1.380\,6509 \times 10^{-23} \text{ J K}^{-1}$, relative standard uncertainty 4.3 ppm) [60] was published. Compared with the first DCGT result [53], the uncertainty has been decreased by more than a factor two, see figure 5. Afterwards the uncertainty was reduced further to 4.0 ppm [48] by reanalysing the pressure measurement [58]. Since 2013, based on a huge amount of data, two new values of the Boltzmann constant k have been obtained by DCGT applying two different highly-stable tungsten-carbide capacitors. The most recent results have been combined with the value published in 2013 [60]. After all correlations have been considered, the final result is $k = 1.380\,6482 \times 10^{-23} \text{ J K}^{-1}$ with a relative standard uncertainty of 1.9 ppm [52]. The reduction of the uncertainty of the final result by a further factor two compared with the result published in 2013 has been mainly achieved by three advances: (i) improvement of the mounting of the capacitor electrodes and attenuation of the influence of stray fields by additional shielding, which led to a better stability and thus a smaller Type A uncertainty component for the two new capacitors; (ii) determination of the individual adiabatic compressibility of the electrodes from the carefully analysed density dependence, which resulted in an essentially smaller uncertainty of the effective compressibility especially for one of these capacitors; (iii) inclusion of many more experimental results by combining the data obtained for three different capacitors in two measurement campaigns.

5. Johnson noise thermometer

5.1 Introduction

Johnson noise thermometers (JNT) determine the thermodynamic temperature from measurements of the fluctuating voltage or current noise caused by the thermal motion of electrons that occurs in all electrical conductors [61, 62]. For temperatures near 300 K and frequencies below 10 MHz, the mean-square voltage of Johnson noise is described by Nyquist's law with a relative error of less than 1×10^{-9} ,

$$\overline{V_T^2} = 4kTR\Delta f, \quad (3)$$

where R is the resistance of the sensor, and Δf is the bandwidth over which the noise is measured [63, 64]. In principle, k can be determined directly by measuring the fluctuating voltage across a sensing resistor at the temperature of the TPW, upon which the temperature unit, kelvin, is presently defined. However, the measurement is extremely challenging because the noise voltage is small ($\sim 1.2 \text{ nV}/\sqrt{\text{Hz}}$), random, and must be measured over very wide bandwidths for very long periods.

Noise thermometers used for metrological applications are all based on the switching correlator design pioneered by Brixy [65, 66]. The design incorporates several features essential for a high-accuracy measurement; the correlator eliminates the uncorrelated noise from the preamplifiers and lead-wires, frequent switching between the measured noise source and a reference noise source eliminates the effects of drifts in the gain and frequency response of the thermometer, and the correlator has a natural four-wire definition of the sensing resistance. Digital versions of the thermometer, with the analogue multiplier replaced by analogue-to-digital converters (ADC) and software multiplication, have the additional benefits of greater accuracy, frequency domain processing with digital definition of the bandwidth, and compact data storage in the form of averaged power spectra [65, 67]. Frequency domain processing also enables several useful diagnostic measurements, including detection of some forms of electromagnetic interference (EMI) [67].

The most significant recent breakthrough was the development, by NIST, of the "quantum accurate voltage noise source (QVNS)" [68-73]. The QVNS provides the means to calibrate the gain and frequency response of the JNT, match the noise powers from the two noise sources to eliminate non-linearity effects, and to match the source impedances of the two noise sources enabling significant increases in bandwidth. The QVNS also simplifies measurements of the non-linearity of the thermometer and its sensitivity to EMI [73-79]. The improvements accompanying the introduction of the QVNS have also made it practical to measure the Boltzmann constant, k . Figure 6 shows a simplified schematic diagram of the QVNS-JNT. If the

amplitudes of the thermal noise voltage and the QVNS voltage are respectively traceable to the quantum Hall effect and the Josephson effect, and the thermal noise source is held at the TPW, the QVNS-JNT measures the ratio of k/h , where h is the Planck constant. The value of k is then determined with practically the same relative uncertainty because the CODATA recommended value of h has much lower relative uncertainty [77].

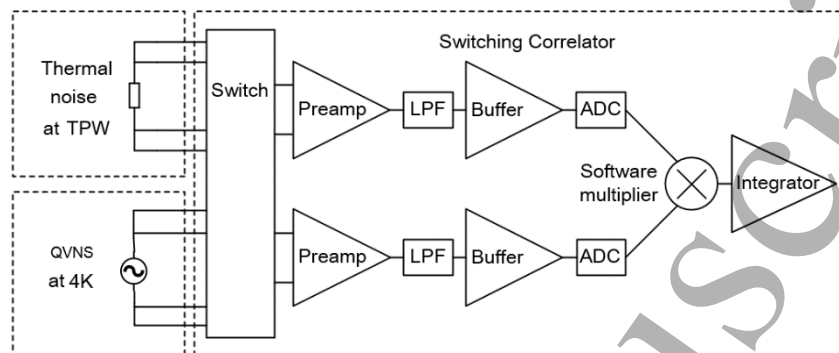


Figure 6. Simplified schematic diagram of a QVNS calibrated JNT. The switch alternately connects the thermal noise source or QVNS to the two amplifier channels that consist of preamplifiers (Preamp), low pass filters (LPF), buffer amplifiers (Buffer), and analogue-to-digital converters (ADC).

In 2011, NIST reported the first practical electronic measurement of the Boltzmann constant, $k = 1.380\,651 \times 10^{-23} \text{ J K}^{-1}$, which was made by comparing the noise of a $100 \text{ } \Omega$ thermal sensor at the TPW with the pseudo-random noise synthesized by a QVNS [77]. The 12.1×10^{-6} combined relative standard uncertainty of this measurement was dominated by two terms: the statistical uncertainty due to the randomness of the noise and a Type B uncertainty related to variations in the frequency dependence of the ratio of the power spectra for the two noise sources. Since then, NIM and NIST have collaborated to develop an additional QVNS-JNT system at NIM to demonstrate the reproducibility of the QVNS-JNT method and to pursue a low uncertainty k determination. The NIM noise thermometer is similar to the design pioneered by NIST [70-79], but with some variations and improvements [80-82]. Most significantly, the system was located in an underground shielded room to reduce EMI. Trimming resistors, capacitors and inductors were inserted in the connecting leads to better match the power spectra of the thermal and QVNS signals. In 2015, by comparing the thermal voltage noise generated by a $200 \text{ } \Omega$ resistor immersed in a TPW cell to a QVNS synthesized pseudo-noise voltage, NIM made a determination of $k = 1.380\,6513 \times 10^{-23} \text{ J K}^{-1}$ with a combined relative standard uncertainty of 3.9×10^{-6} [82]. Again, the dominant contributions to the uncertainty are from the statistical uncertainty and spectral mismatch effects.

5.2 Frequency response mismatch

The major challenge limiting the measurement uncertainty in all recent JNT measurements arises from the different sets of leads connecting the thermal noise source and the QVNS to the

1
2
3 correlator. Since the connecting leads of the two sources are inherently different, it is difficult to
4 match the measured power spectra of the two ideally-white noise signals. Additionally, the two
5 noise sources respond differently to noise currents originating in the preamplifiers and lead-
6 wires, leading to an error that increases with the frequency squared. Any frequency-response
7 mismatch in the sets of lead wires causes a bias in the measurement that rapidly increases with
8 frequency, and therefore limits the bandwidth and the statistical uncertainty. While it is practical
9 to correct the spectral-mismatch bias, the correction is accompanied by a significant increase in
10 the statistical component of uncertainty and there is always some remaining uncertainty due to
11 the imperfection of the model. Whatever model is chosen, the statistical uncertainty decreases
12 with increasing bandwidth, while the systematic uncertainty due to the spectral mismatch
13 increases. More investigations are required to decrease the latter uncertainty.

21 Both NIST and NIM used even-order polynomial functions to model the ratio of the power
22 spectra based on low-frequency filter theory [77, 82]. Physically, the frequency response of the
23 connecting leads can be described by a full transmission-line model, however, for the low
24 frequencies and short lead lengths used in the JNT, time delays can be neglected and a
25 lumped-parameter model is sufficient. Numerical simulations show that the lumped-element
26 model is indistinguishable from a full transmission-line model at frequencies below 1 MHz [83].
27 In the 2011 Boltzmann constant determination at NIST, the measured ratio of the noise power
28 spectra was fitted with a two-parameter model to correct any effects with a square-law
29 dependence on frequency [77]. In the 2015 determination at NIM, the model was expanded to
30 include more terms to eliminate higher-order mismatch effects [82]. The inclusion of additional
31 terms in the data analysis model has the effect of increasing the statistical variance in the
32 measurement, approximately linearly with model order, while rejecting mismatch effects of the
33 selected order. Hence, there is a bias-variance compromise between model complexity and
34 measurement bandwidth that achieves the minimum uncertainty.

43 To select the optimum order of the model and the bandwidth, Coakley and Qu developed a
44 data-driven statistical learning method using cross-validation to optimize the bias-variance
45 compromise [84]. In cross-validation, the observed data is split into training and validation
46 subsets, with candidate models fitted to the training data and tested to identify the model that is
47 most consistent with validation data. This evaluation is repeated with a large number of
48 randomised splits of the training and validation data, to determine selection fractions for each
49 model. Based on the selection fractions, the cross-validation algorithm calculates an uncertainty
50 of the determined k that accounts for both random effects due to the measurement of noise and
51 systematic effects associated with imperfect knowledge of the model. The process is also
52 repeated for different bandwidths to select the thermometer bandwidth that minimizes the total
53 uncertainty. The cross-validation algorithm has an important feature of producing an objective
54
55
56
57
58
59
60

1
2
3 estimate of the uncertainty due to the connecting-lead mismatch effects. The method was first
4 demonstrated with the analysis of the NIM 2015 data [84].
5

6
7 With the 2017 measurement at NIM, additional physical modelling of the connecting leads
8 between noise sources and the correlator was carried out [83]. A term-by-term comparison of
9 the transfer functions indicates that to get the same frequency response for the two noise
10 signals, the connecting leads for the thermal and QVNS noise sources should ideally be
11 identical, and the resistors on each of the QVNS output lead should be of the same resistance
12 as that of the thermal sensor. Furthermore, the analysis indicates that trimming components
13 placed in the wrong place might create complex spectral features that could not be fitted well by
14 low-order models. Another difficulty was the changing inductance of the leads with temperature
15 and frequency, which made the close match of the leads problematic. These effects were
16 eventually traced to the skin effect [84].
17
18
19
20
21
22

23 Several changes were made to the NIM noise thermometer to reduce frequency-response-
24 mismatch effects [85]. Firstly, the connecting leads between the noise sources and the
25 measurement circuits used a coaxial arrangement to better define the inductance and
26 capacitance of the leads. Secondly, to minimise the effects of different temperatures on the
27 cable impedances, very thin coaxial cable with solid beryllium-copper conductors and foam
28 dielectric was used. Thirdly, better matching of the frequency response for the two noise
29 sources was achieved by using identical length coaxial cables. No additional trimming inductors
30 or capacitors were used. The sensing resistance was also reduced from 200 Ω to 100 Ω to
31 improve the impedance match with the 50 Ω cables and to further flatten the frequency
32 response. Possible effects due to noise currents induced by the dielectric loss in stray
33 capacitance associated with the switch and preamplifier were substantially reduced by replacing
34 the fiberglass printed circuit boards (PCBs) with Teflon composite PCBs.
35
36
37
38
39
40
41
42

43 *5.3 Latest Measurements*

44
45 With the improved JNT system, NIM performed a new measurement of k in 2017 [85]. Although
46 the bandwidths did not increase compared to the 2015 measurement, the results of analyses
47 with the different order models are much more consistent with each other, as shown in figure 7,
48 yielding a significant reduction in the uncertainty due to spectral mismatch. Combined with
49 reduced statistical uncertainty due to a longer integration period of 100 days, the new
50 measurement achieved an improved determination of $k = 1.380\ 6497 \times 10^{-23} \text{ J K}^{-1}$ with a relative
51 standard uncertainty of 2.7×10^{-6} . The combined relative uncertainty of less than 3×10^{-6} met the
52 CCT's second requirement for proceeding with the redefinition of the kelvin [2, 86].
53
54
55
56
57

58 NIST also performed a new determination of k in 2017 [87]. The differences between the new
59 NIST measurement and the other measurements are the value of the sense resistor as well as
60

both the circuit and procedure used to match the transfer functions. The sense resistance was increased from $100\ \Omega$ to $200\ \Omega$ to increase the signal-to-noise ratio. Most importantly, NIST used trimming components and a multi-step procedure to tune the electrical circuit and reduce the frequency dependence of the ratio of the power spectra for all frequencies up to 1 MHz. An additional switchboard was used to dynamically adjust the grounding conditions. Compared to earlier NIST measurements, the shielding was dramatically improved to reduce EMI. With this significantly modified system, NIST reported the determination of $k = 1.380\ 6429 \times 10^{-23}\ \text{J K}^{-1}$ with a relative combined standard uncertainty of 5.0×10^{-6} from 50 days of accumulated data.

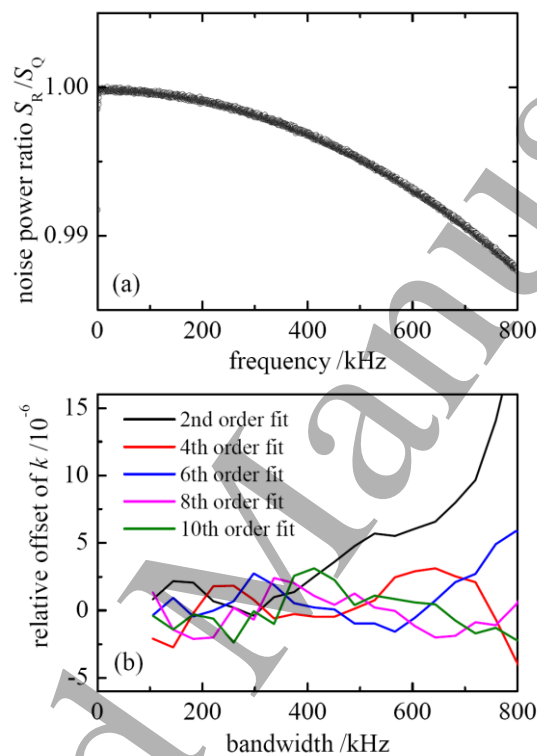


Figure 7. (a) The noise power ratio spectrum from the NIM 2017 measurements, where S_R and S_Q are the measured power spectral densities of thermal noise and quantum voltage noise, respectively, and (b) the estimate of relative offset of k from CODATA recommended value versus bandwidth and order of the even-order polynomial fit.

The National Measurement Institute of Japan (NMIJ/AIST) has also been developing a JNT, with the same basic principles as the NIST system [88]. A key distinguishing feature is the integrated quantum voltage noise source (IQVNS), which is a conventional shift-register based pseudo-random number generator but fully implemented with superconducting integrated circuits. The driving method for the Josephson junction array differs from that of either NIST or NIM. Also, rather than using cross validation to optimise the model selection and bandwidth, NMIJ adopted the Akaike information criterion to select the lower- and the upper-cut-off frequencies for use with a quadratic spectral-correction model. With about 5 days accumulated data, the final result is $k = 1.380\ 643\ 6 \times 10^{-23}\ \text{J K}^{-1}$ with a relative combined standard uncertainty of 10.2×10^{-6} .

6. Doppler broadening thermometer

The Doppler broadening technique (DBT) was first proposed in 2002 [89]. A molecular (or atomic) absorption line of a gas at thermodynamic equilibrium exhibits a Doppler broadened profile which reflects the Maxwell-Boltzmann velocity distribution of gas particles. In conjunction with some highly accurate modeling of the line profile, it is possible to use the data to retrieve the e-fold half-Doppler width $\Delta\nu_D$, whose relation to k is given by:

$$k = \frac{mc^2}{2T} \left(\frac{\Delta\nu_D}{\nu_0} \right)^2 \quad (4)$$

where ν_0 is the central frequency of the molecular line, c is the speed of light, T is the temperature of the gas and m its molecular mass. Thus, DBT consists of accurately and simultaneously measuring the temperature and line shape. k is then calculated from Equation (4).

In order to extract the Doppler component of the width, the measured line shape is fitted to a physical model. The choice of model is critical and is an intricate problem. The absorption line shape of a single rovibrational molecular line is dominated at very low pressure by the inhomogeneous Doppler broadening and is a simple Gaussian profile. In practice however, collisions induce both an additional broadening and a shift. The overall line shape is then a Voigt profile (VP), i.e. the convolution of the above mentioned Gaussian profile with a Lorentzian profile. The line shape can be further refined by taking into account speed-dependent and Lamb-Dicke-Mössbauer narrowing effects. Depending on the assumption made for molecular collisions (hard or soft collisions), adding these contributions to the VP leads to different profiles.

6.1 Results obtained at Laboratoire de Physique des Lasers

At the Laboratoire de Physique des Lasers (LPL), the DBT was used to measure k by carrying out laser spectroscopy of an ammonia rovibrational line at 10.35 μm [90]. The absorption line probed is the ν_2 saQ(6,3) rovibrational line of the $^{14}\text{NH}_3$ ammonia molecule of frequency $\nu = 28\,953\,693.9(1)$ MHz. This well-isolated transition has been chosen to avoid any deformation of the profile due to line mixing with neighbouring lines. Owing to the non-zero spin values of the nitrogen and hydrogen nuclei, an unresolved hyperfine structure is present in the Doppler profile. This hyperfine structure has been recorded by saturation spectroscopy to determine the induced broadening of the absorption linewidth, recorded in linear absorption, and its impact on the Doppler width measurement [91].

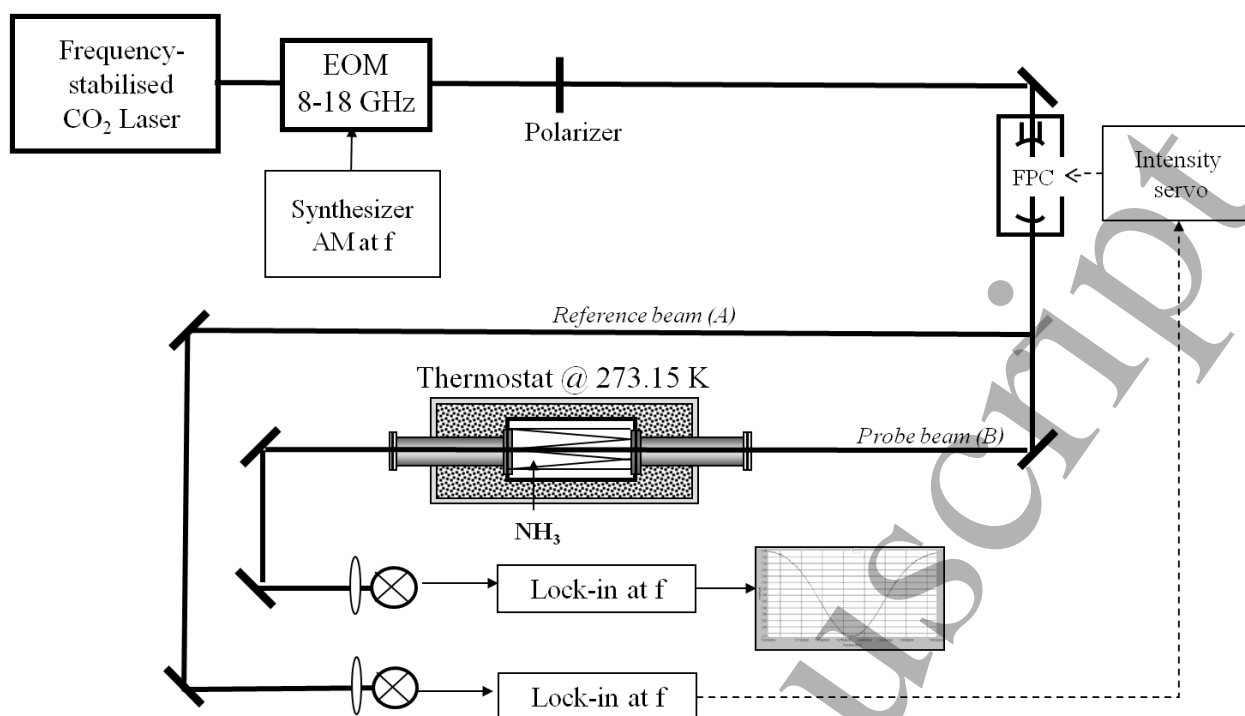


Figure 8. Experimental setup used at Laboratoire de Physique des Lasers (AM: Amplitude Modulation, EOM: Electro-Optic Modulator, FPC: Fabry Perot Cavity, Lock-in: Lock-in Amplifier).

The experimental setup is shown in figure 8. The laser source, a frequency stabilized CO₂ laser emitting around 10 μm , exhibits a spectral width smaller than 10 Hz and a frequency stability of 0.1 Hz for a 100 s integration time [92]. The CO₂ laser source is coupled to a microwave (MW) electro-optic modulator (EOM) which generates tuneable sidebands from 8 GHz to 18 GHz on both sides of the fixed laser frequency. After the MW EOM, a grid polarizer and a Fabry-Perot cavity (FPC) are used to filter out the residual carrier and the unwanted sideband. The FPC is also used to stabilize the intensity of the transmitted reference beam (A). The probe beam (B) feeds an ammonia absorption cell for spectroscopy. The absorption length of the cell can be adjusted from 37 cm in a single pass configuration to 3.5 m in a multi-pass configuration. For noise filtering, both reference (A) and probe (B) beams are amplitude-modulated at $f = 40$ kHz via the (8-18) GHz EOM and then demodulated with a lock-in amplifier. The sideband is tuned close to the molecular resonance and scanned to record the absorption profile. This experiment requires the molecular gas to be maintained at a constant and homogeneous temperature. The absorption cell is placed inside a copper thermal shield which is itself inside a stainless steel enclosure immersed in a thermostat filled with an ice-water mixture which stabilizes the temperature close to 273.15 K. The temperature is measured with glass capsule-type standard platinum resistance thermometers placed on the absorption cell. The thermostat and temperature chain, and their performance, are described in detail in references [93, 94].

In 2007, LPL in collaboration with LNE-CNAM undertook a first proof-of-principle experiment. k was determined with a combined relative uncertainty of 190×10^{-6} leading to $k = 1.380\,65 \times 10^{-23} \text{ J K}^{-1}$ [90]. At that time, the spectral analysis was performed using a simple

1
2
3 Gaussian profile. In the last decade, major technical improvements and upgrades of the
4 spectrometer have been accompanied by an increasingly refined interpolation of the
5 experimental profiles [95, 96]. At present, the most accurate value for the Boltzmann constant
6 that can be deduced from the DBT at LPL is $k = 1.380\,704 \times 10^{-23} \text{ J K}^{-1}$ showing a combined
7 uncertainty of 50 ppm [91]. This result has been confirmed after a complete analysis of the line
8 shape considering a speed-dependent hard-collision model (and establishing for the first time
9 the speed dependent Galatry profile as the profile of choice for the NH_3 line considered in our
10 pressure range) including hyperfine structure and detection-bandwidth-induced line shape
11 distortions [96, 97].

12
13
14 Recently, the LPL has developed a new spectrometer based on a widely tunable quantum
15 cascade laser [98]. As a result of the higher available intensity and the potentially lower
16 amplitude noise of quantum cascade lasers, a large reduction in the time needed to record
17 absorption spectra is expected. Furthermore, the increased intensity range available allows
18 power-related systematic effects to be studied for the first time. In particular, it has allowed the
19 first evaluation of the saturation parameter of the probed transition and its impact on the
20 determination of k [97]. Finally, by investigating and improving the control over a variety of
21 systematic effects (those mentioned above and others), it has been demonstrated that in theory
22 a measurement of k at a 2.3 ppm accuracy level is reachable using the DBT on ammonia [97].

33 *6.2 Results obtained at Università degli Studi della Campania*

34
35 Doppler broadening thermometry has been implemented at Università degli Studi della
36 Campania “Luigi Vanvitelli” (formerly, Seconda Università degli Studi di Napoli) for roughly one
37 decade, in cooperation with INRiM. So far, three molecular targets have been employed: CO_2 ,
38 H_2^{18}O and C_2H_2 [99]. Three generations of spectrometer have been designed and implemented,
39 with increasing complexity. The main difference, as compared to the French experiments,
40 consists in the choice of the wavelength region. In particular, the near-infrared (NIR) region has
41 been preferred because of the excellent performance of indium–gallium–arsenide (InGaAs)
42 detectors, in terms of linearity of the response and noise level.

43
44 There were two spectroscopic determinations of the Boltzmann constant, namely
45 $1.380\,58(22) \times 10^{-23} \text{ J K}^{-1}$ and $1.380\,631(33) \times 10^{-23} \text{ J K}^{-1}$. The former was obtained as a result
46 of a proof-of-principle experiment, by means of an absorption spectrometer based on an
47 extended-cavity diode laser at 2- μm wavelength to interrogate a vibration–rotation transition of
48 carbon dioxide [100]. More particularly, the shape of the well isolated R(12) component of the
49 $\nu_1 + 2\nu_2^0 + \nu_3$ band was probed at different temperatures, between the triple point of water and
50 the gallium melting point.

51
52 The latter resulted from a dual-laser water spectrometer operating at 1.39 μm [101] and it is still
53 the most accurate determination ever performed by means of an optical method, the combined

relative uncertainty being 24 parts in 10^6 . The complete uncertainty budget was first illustrated in reference [102] and then further refined in reference [103], while hyperfine structure effects arising from the nuclear spin of the two hydrogen atoms have been discussed and quantified only recently [104]. The major sources of uncertainty are due to: i) the statistical fluctuation of the data points arising from individual fits of repeated spectra; ii) the spectral purity of the probe laser; iii) the line shape model.

In the first determination, the spectral analysis was performed by using a Voigt profile. In fact, even in the Doppler regime, the absorption profile is perturbed by binary collisions that lead to an additional broadening of the spectral line. Nevertheless, depending on the experimental precision, narrowing effects can be observed, typically due to the joint occurrence of two phenomena: the speed dependence of collision relaxation rates and the averaging effect of velocity-changing collisions. These effects have been carefully considered in the second-generation experiment, by adopting a very sophisticated line shape model, known as partially correlated speed-dependent hard-collision model.

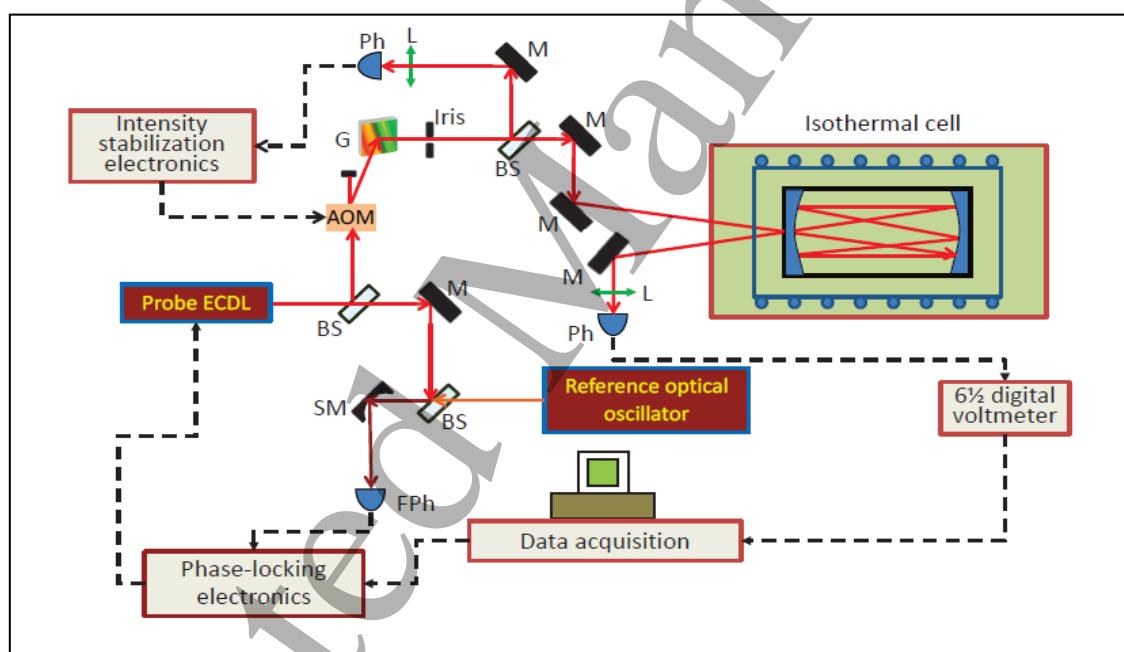


Figure 9. Schematic diagram of the third-generation spectrometer developed at Università degli Studi della Campania. ECDL stands for extended-cavity diode laser, M for mirror, SM for spherical mirror, L for lens, BS for beam splitter, Ph for photodiode, FPh for fast photodiode, G for grating, AOM for acousto-optic modulator. The reference optical oscillator is directly linked to an optical frequency comb synthesizer. The probe ECDL is phase locked to the reference oscillator, with a tunable offset frequency. The intensity of the probe beam is actively stabilized.

Very recently, a third-generation experiment has been performed, implementing several technical upgrades to the water spectrometer and adopting a new molecular target, namely, acetylene (C_2H_2), which shows interesting absorption features at $1.39 \mu m$ [105, 106]. This choice offers some important advantages, as compared to water, C_2H_2 being a non-polar and linear molecule. A sketch of the new spectrometer is illustrated in figure 9. Doppler width

retrieval from line fitting is also improved significantly. Differently from previous works, in which individual fits were performed, a global analysis approach has been implemented and applied to simultaneously fit a manifold of experimental profiles (acquired at the same temperature) across a given range of pressures, sharing a restricted number of unknown parameters, including the Doppler width. As explained elsewhere [107], the global analysis reduces the uncertainty associated to the line shape model as well as the fluctuations resulting from statistical correlations among free parameters. Recent results demonstrate that low uncertainty determinations are possible. The main limitation of this latter experiment is the signal-to-noise ratio in the spectral acquisitions. The isothermal cell consists in a spherical, Herriott-type, multiple reflection cell with a maximum path-length of 12 m. The use of a long-path technique has been one of the novelties with respect to the previous experiments. It has been necessary to compensate for the small line intensities of acetylene at 1.39 μm . The partial overlapping of the reflected beams inside the cell gives rise to interference fringes that perturb the absorption spectra. This limitation, which can be overcome with a few technical expedients to be implemented on the cell itself, has prevented the Italian team to improve the spectroscopic determination of the Boltzmann constant. Nevertheless, the perspective of improving DBT so as to make possible temperature determinations with an uncertainty level around 10 parts per million is concrete and feasible in the near future.

7. Consequences of the redefinition

The current definition of the kelvin, valid since 1954, defines the temperature unit kelvin via a material property of a special substance. The kelvin is the 273.16th part of the thermodynamic temperature of the triple point of water [108]. Thus, influences of the isotope composition and the purity of the water used are of critical importance for their practical realisation. Thereby, the long-term stability is jeopardized over space and time. By determining the Boltzmann constant, this defect is remedied.

The new definition of the kelvin based on the methods described above will be as follows [109]: The kelvin, symbol K, is the SI unit of thermodynamic temperature. It is defined by taking the fixed numerical value of the Boltzmann constant k to be $1.380\,649 \times 10^{-23}$ when expressed in the unit J K^{-1} , which is equal to $\text{kg m}^2 \text{s}^{-2} \text{K}^{-1}$ (explicit definition of a fundamental constant). One kelvin is thus the change of the thermodynamic temperature T which corresponds to a change of the thermal energy kT of $1.380\,649 \times 10^{-23}$ joule. This formulation is in analogy to the current definition of the meter and can be considered as an explicit definition of the unit itself. In effect, both formulations are equivalent. Strictly speaking, a unit of temperature of its own would no longer be necessary; however, all thermometers would then

1
2
3 have to indicate the joule. For many reasons, this approach is not feasible, practical or
4 enforceable. But what are the consequences of such a new definition?
5

6
7 Initially, the consequences will be of importance only for precision metrology, not in everyday
8 use. Only in this way can international metrology function in an undisturbed way, and the
9 world economy will not be affected. To achieve this, the CCT has prepared a recommendation
10 for implementation (*mise en pratique*) of the new definition. The *mise en pratique* includes
11 recommendations for the direct measurement of the thermodynamic temperature T . Texts
12 defining the International Temperature Scales ITS-90 and PLTS-2000, which will remain valid,
13 supplement this [15]. The recommendation for the implementation will also discuss the
14 differences $T-T_{90}$ and $T-T_{2000}$ of these two defined scales with the respective uncertainties.
15
16 The temperature values of T_{90} and T_{2000} will thereby be measured in accordance with the
17 requirements of ITS-90 and PLTS-2000.
18
19
20
21
22

23 This approach allows direct thermodynamic temperature measurements far away from the
24 triple point of water. These are, for example, high temperatures where the radiation
25 thermometer can be used as interpolation instrument of the ITS-90, but in future also as
26 primary thermometer [110]. At the highest temperature fixed points of the ITS-90, at 1300 K, for
27 example, the uncertainties are about one thousand times larger than the reproducibility of the
28 TPW, approximately 30 μ K. These uncertainties can be considerably reduced in the future by
29 means of primary radiation thermometers. Thus, there are significant benefits of the new
30 definition of the kelvin, particularly for temperature measurements below ~ 20 K and above
31 ~ 1300 K, where primary thermometers may offer a lower thermodynamic uncertainty than is
32 currently available with the defined International Temperature Scales. In the future, as the
33 primary methods evolve and achieve lower uncertainties, they will become more widely used
34 and may gradually replace the defined scales as the basis of temperature measurement.
35
36
37
38
39
40
41

42 Note that the fixed-point temperatures assigned in all of the defined scales are exact with
43 respect to the respective scale temperature (there is no assigned uncertainty) and fixed (the
44 value remains unchanged throughout the life of the scale). As a consequence, the redefinition
45 of the kelvin in terms of the Boltzmann constant has no effect on the temperature values or
46 realisation uncertainties of the present two defined scales. In particular, the status of the TPW
47 as a fixed point, with a defined temperature value on the ITS-90, will remain unchanged. Thus,
48 the uncertainty of realisation of the TPW on the ITS-90 will not acquire any additional
49 uncertainty due to the change in definition. In the temperature range around the triple point of
50 water, which is important in practice, the ITS-90 will still keep its right to exist as it will also in
51 future be of great importance for the worldwide harmonization of temperature measurement.
52
53 The uncertainty of its realisation is currently still up to one order of magnitude lower than the
54 uncertainty of the thermodynamic temperature T . However, the TPW, which is currently - by
55
56
57
58
59
60

1
2
3 definition - provided with an exact temperature, will lose this unique status. It will then be a
4 temperature fixed point like any other, which has exactly the same uncertainty as the
5 Boltzmann constant at the time of its fixing. The relative uncertainty of 3.7×10^{-7} then
6 corresponds to an uncertainty of 0.10 mK for the thermodynamic temperature of the TPW.
7
8
9

10 11 12 **8. Conclusion**

13
14 The starting point for determinations of the Boltzmann constant leading to a new definition of
15 the kelvin was the EURAMET project 885 and a funded iMERAPlus research project. Between
16 2008 and early 2011 this project [10] was coordinating the European activities to determine k in
17 Denmark (Danish Fundamental Metrology, DFM), France (Laboratoire National de Métrologie
18 et d'Essais, LNE-CNAM, and Laboratoire de Physique des Lasers at University Paris North,
19 LPL), Italy (Istituto Nazionale di Ricerca Metrologica, INRiM, and Universities of Naples and
20 Milan), Spain (Universidad de Valladolid and Centro Español de Metrología, CEM), United
21 Kingdom (National Physical Laboratory, NPL) and Germany (Physikalisch-Technische
22 Bundesanstalt, PTB). This large research collaboration resulted in a major progress and overall
23 in essential developments for AGT. The AGT measurements of LNE-CNAM [33, 34], NPL
24 [111], and INRiM [112] all used resonators jointly developed within the iMERAPlus project and
25 achieved then the smallest uncertainties of all methods. All results were highly consistent and
26 agreed very well with the CODATA value of 2006 [9] based mainly on [6]. These four new
27 determinations were exploited by the CODATA TGFC in its 2010 adjustment together with the
28 fundamental AGT results [6] and [5]. The CODATA TGFC recommended a value for k with a
29 relative standard uncertainty of 9.1×10^{-7} [11].
30
31
32
33
34
35
36
37
38
39

40 The development of the various experiments in terms of the published uncertainties is
41 reviewed in table 3. As shown in the table, there are now several determinations of k by AGT
42 featuring a relative standard uncertainty around 1×10^{-6} . Because of these and because the
43 discrepancy between LNE-11 and NPL-13 experiments is resolved, the relative standard
44 uncertainty of the adjusted value of k was already in the 2014 CODATA adjustment only
45 5.7×10^{-7} [12]. This uncertainty is securely below 1.0×10^{-6} thus fulfilling the first CCT condition
46 for the new definition of the kelvin [2]. The uncertainties of all determinations taken into
47 account in the 2014 CODATA adjustment are marked in bold.
48
49
50
51
52
53
54
55
56
57
58
59
60

Table 3. Development of the relative standard uncertainties $u(k)/k$ of high-accuracy determinations of the Boltzmann constant. Applied method and gas are specified. The uncertainties of the determinations contributed to the 2014 CODATA adjustment are marked in bold. The correlations among all AGT measurements are considered as derived in refs. [13, 113]. New determinations after the CODATA 2014 adjustment with uncertainties in italics.

determination	method	gas	$(u(k)/k) / 10^{-6}$			
			up to 2011	2013	2015	2017
NIST-88	AGT	Ar	1.77	-	-	-
INRiM-10, -15	AGT	He	7.49	-	<i>1.06</i>	-
LNE-09, -15, -17	AGT	He	2.73	-	1.01	<i>0.60</i>
LNE-11	AGT	Ar	1.41	-	-	-
NPL-10, -13, -17	AGT	Ar	3.19	0.90	-	<i>0.70</i>
UVa/CEM-15, -17	AGT	Ar	-	-	20	6.7
NIM-11, -13, -17	c-AGT	Ar	7.9	3.70	-	2.0
PTB-11, -13, -15, -17	DCGT	He	7.9	4.3	4.0	<i>1.94</i>
NIM/NIST-15, -17	JNT	-	-	-	3.9	<i>2.71</i>
NIST-11, -17	JNT	-	12.1	-	-	<i>5.0</i>

In addition, the recent low-uncertainty determinations INRiM-15 [25], PTB-17 [52], NIM/NIST-17 [85], NPL-17 [46], LNE-17 [26], NIM-17 [27], UVa/CEM-17 [29] and NIST-17 [87] are listed in table 3 with uncertainty values in italics. With the DCGT result PTB-17 [52] and the noise result NIM/NIST-17 [85], the second CCT condition [2], demanding an independent method with a relative standard uncertainty below 3×10^{-6} , is fulfilled. Thus, the way for the new definition of the kelvin is free. In figure 10, apart from the determinations listed in table 3, also the CODATA adjusted values of 2010 [11] and 2014 [12] are shown for comparison.

For clarity, in figure 11 only those determinations are repeated, which contributed to the final 2017 special adjustment of the CODATA TGFC [13] to be used for the redefinition of the kelvin. In the figure, all four measurements of LNE are combined to the mean value taken from appendix B of ref. [26]. The blue confidence band ($\pm 3.7 \times 10^{-7}$) of the adjusted CODATA value of 2017 ($k = 1.380\,649\,03 \times 10^{-23} \text{ J K}^{-1}$) demonstrates the excellent agreement of all contributing results. As well the CODATA adjusted values of 2014 [12] and 2017 [13] are in remarkable agreement, corresponding to a difference in temperature of only 0.10 mK.

Our review of the Boltzmann project reveals that the development of primary thermometers made considerable progress. Therefore, an adjusted value was achieved for the Boltzmann constant k with a relative standard uncertainty of only 3.7×10^{-7} , which is based on various experiments with three different methods: the acoustic gas thermometer (AGT), the dielectric-

1
2
3 constant gas thermometer (DCGT) and the Johnson noise thermometer (JNT) (figure 11).
4 Besides, the Doppler broadening thermometer (DBT) was able to provide an additional
5 confirmation, though with larger uncertainties.
6
7

8 By fixing the numerical value of the Boltzmann constant once for all in 2018, the redefinition of
9 the kelvin is affected. In this way, a fundamental constant rather than a specified substance will
10 become the reference for temperature. Any thermodynamic temperature can in principle be
11 realized without the necessity of starting all traceability from a single fixed point. Perhaps most
12 important, future improvements in thermometry techniques will not lead to another redefinition
13 of the kelvin. The essential consequences are of a long-term nature, as the measuring system
14 for the temperature would thus be infinitely stable. This objective was worth the effort made
15 world-wide.
16
17
18
19
20
21
22
23
24
25
26
27
28
29
30
31
32
33
34
35
36
37
38
39
40
41
42
43
44
45
46
47
48
49
50
51
52
53
54
55
56
57
58
59
60

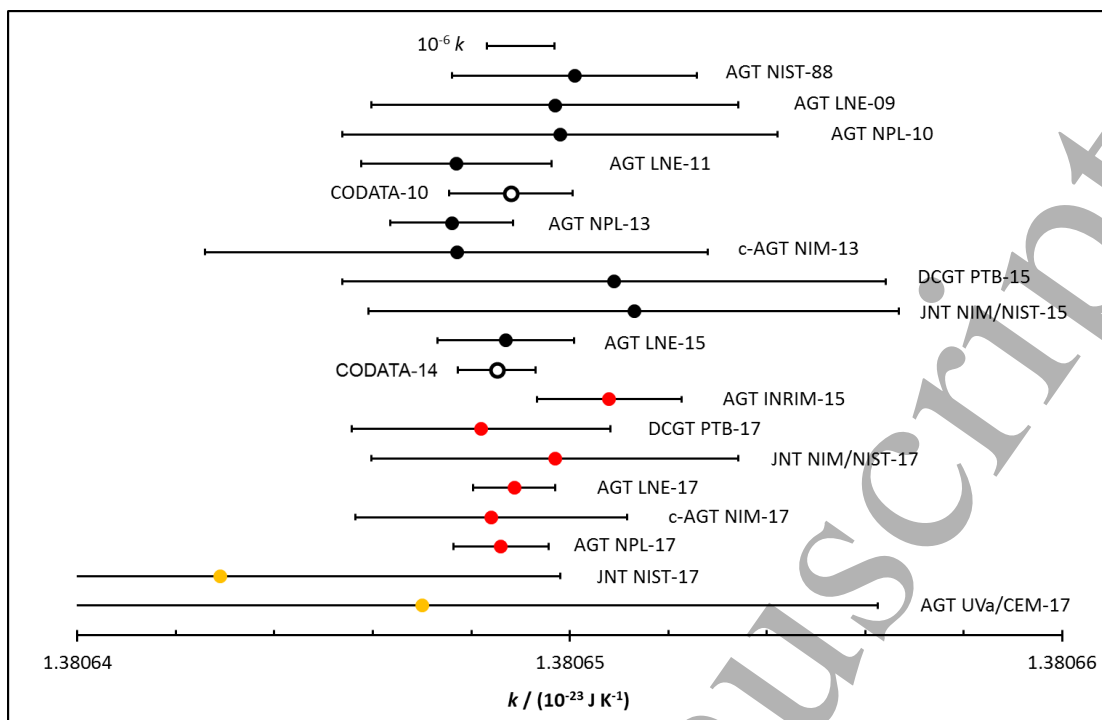


Figure 10. Determinations of the Boltzmann constant in chronological order. Black dots: all contributions to the adjusted CODATA value of 2014. Red dots: new measurements contributing to the CODATA 2017 adjustment. The uncertainties of the recent determinations UVa/CEM-17 with AGT and NIST-17 with JNT did not meet the CODATA TGFC criterion for inclusion in the adjustment (yellow dots). In addition, the CODATA adjusted values of 2010 and 2014 are shown as open circles. All bars denote standard uncertainties.

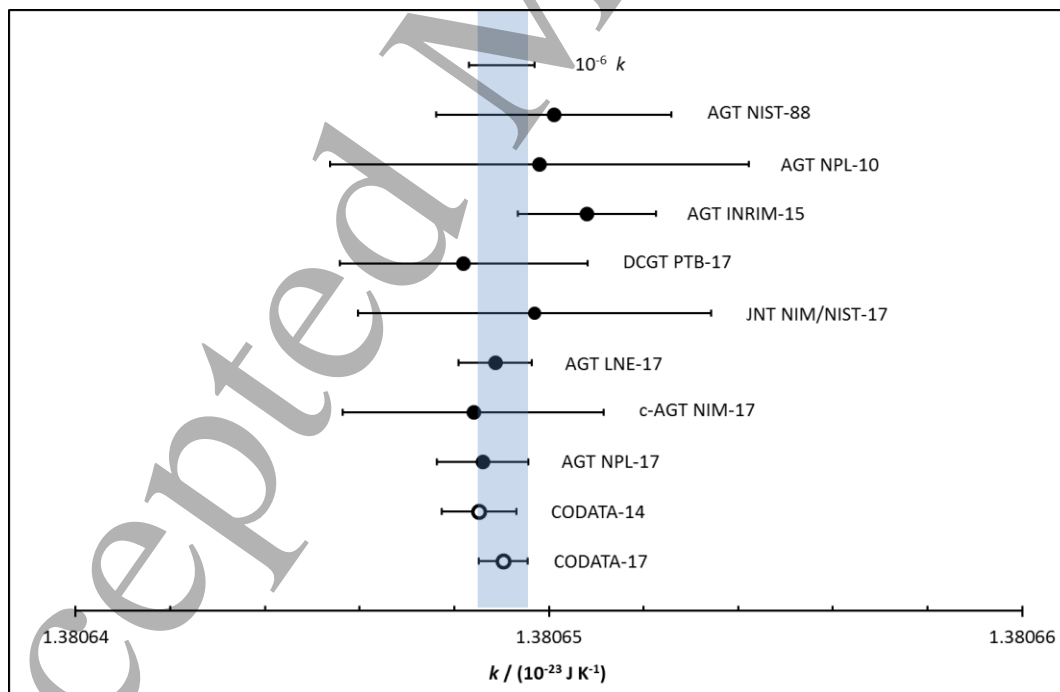


Figure 11. All determinations of the Boltzmann constant contributing to the adjusted CODATA value of 2017. For clarity, all four results of LNE have been combined to a mean value [26]. In addition, the CODATA adjusted values of 2014 [12] and 2017 [13] are shown as open circles. All bars denote standard uncertainties and the blue band that of the 2017 CODATA value.

References

- [1] A. Einstein 1905 Über die von der molekularkinetischen Theorie der Wärme geforderte Bewegung von in ruhenden Flüssigkeiten suspendierten Teilchen *Ann. Phys.* **17** 549-560
- [2] Consultative Committee for Thermometry (CCT) 2014 Report of the 27th meeting, Recommendation CCT T1 <http://www.bipm.org/utils/common/pdf/CC/CCT/CCT27.pdf>
- [3] Cohen E R and Taylor B N 1973 The 1973 Least-Squares Adjustment of the Fundamental Constants *J. Phys. Chem. Ref. Data* **2** 663-734
- [4] Cohen E R and Taylor B N 1987 The 1986 adjustment of the fundamental physical constants *Rev. Mod. Phys.* **59** 1121-1148
- [5] Colclough A R, Quinn T J and Chandler T R D 1979 An acoustic redetermination of the gas constant *Proc. R. Soc. Lond. A* **368** 125–139
- [6] Moldover M R, Trusler J P M, Edwards T J, Mehl J B and Davis R S 1988 Measurement of the universal gas constant R using a spherical acoustic resonator *J. Res. Natl. Bur. Stand.* **93** 85-144
- [7] Mohr P J and Taylor B N 2000 CODATA recommended values of the fundamental physical constants: 1998 *Rev. Mod. Phys.* **72** 351-495
- [8] Mohr P J and Taylor B N 2005 CODATA recommended values of the fundamental physical constants: 2002 *Rev. Mod. Phys.* **77** 1-107
- [9] Mohr P J, Taylor B N and Newell D B 2008 CODATA recommended values of the fundamental physical constants: 2006 *Rev. Mod. Phys.* **80** 633–730
- [10] Fischer J, Fellmuth B, Gaiser C, Zandt T, Pitre L, Briauudeau S, Sparasci F, Truong D, Hermier Y, Gavioso R M, Guianvarc'h C, Giuliano Albo P A, Merlone A, Moro F, de Podesta M, Sutton G, Underwood R, Machin G, Del Campo D, Segovia Puras J, Vega Maza D, Petersen J, Hald J, Nielsen L, Valkiers S, Darquié B, Bordé C, Chardonnet C, Daussy C, Gianfrani L, Castrillo A, Laporta P and Galzerano G 2013 The IMERAPlus joint research project for determinations of the Boltzmann constant, C W Meyer (Ed.) *Temperature: Its Measurement and Control in Science and Industry*, vol 8, AIP Proceedings, New York **1552** 1-10
- [11] Mohr P J, Taylor B N and Newell D B 2012 CODATA recommended values of the fundamental physical constants: 2010 *Rev. Mod. Phys.* **84** 1527–1604
- [12] Mohr P J, Newell D B and Taylor B N 2016 CODATA recommended values of the fundamental physical constants: 2014 *Rev. Mod. Phys.* **88** 035009
- [13] Newell D B, Cabiati F, Fischer J, Fujii K, Karshenboim S G, Margolis H S, de Mirandés E, Mohr P J, Nez F, Pachucki K, Quinn T J, Taylor B N, Wang M, Wood B M and Zhang Z 2017 The CODATA 2017 Values of h , e , k , and N_A *Metrologia* **54** accepted, doi.org/10.1088/1681-7575/aa950a
- [14] Fellmuth B, Gaiser C and Fischer J 2006 Determination of the Boltzmann Constant – status and prospects *Meas. Sci. Technol.* **17** R145-R159
- [15] Fellmuth B, Fischer J, Machin G, Picard S, Steur P, Tamura O, White R and Yoon H 2016 The kelvin redefinition and its mise en pratique *Phil. Trans. R. Soc. A* **374** 20150037
- [16] Moldover M, Gavioso R M, Mehl J B, Pitre L, de Podesta M and Zhang J T 2014 Acoustic gas thermometry *Metrologia* **51** R1-R19
- [17] Mehl J B and Moldover M R 1986 Measurement of the ratio of the speed of sound to the speed of light *Phys. Rev.* **A34** 33481-3344
- [18] Mehl J B, Moldover M R and Pitre L 2004 Designing quasi-spherical resonators for acoustic thermometry *Metrologia* **41** 295–304
- [19] Mehl J B 2007 Acoustic eigenvalues of a quasispherical resonator: Second order shape perturbation theory for arbitrary modes *J. Res. Natl. Inst. Stand. Technol.* **122** 163-173
- [20] Mehl J B 2009 Second-order electromagnetic eigenfrequencies of a triaxial ellipsoid *Metrologia* **46** 554–559
- [21] Edwards G and Underwood R 2011 The electromagnetic fields of a triaxial ellipsoid calculated by modal superposition *Metrologia* **48** 114-122

- [22] Underwood R, Flack D, Morantz P, Sutton G, Shore P and de Podesta M 2011 Dimensional characterization of a quasispherical resonator by microwave and coordinate measurement techniques *Metrologia* **48** 1-15
- [23] Aziz R A, Janzen A R and Moldover M R 1995 Ab initio Calculations for helium: a standard for transport property measurements *Phys. Rev. Lett.* **74** 1586-1589 and Cencek W, Przybytek M, Komasa J, Mehl J B, Jeziorski B and Szalewicz, K 2012 Effects of Adiabatic, Relativistic, and Quantum Electrodynamics Interactions on the Pair Potential and Thermophysical Properties of Helium *J. Chem. Phys.* **136** 224303
- [24] Vogel E, Jäger B, Hellmann R and Bich E 2010 Ab initio pair potential energy curve for the argon atom pair and thermophysical properties for the dilute argon gas. II. Thermophysical properties for low-density argon *Molecular Physics* **108** 3335–3352
- [25] Gavioso R M, Madonna Ripa D, Steur P P M, Gaiser C, Truong D, Guianvarc'h C, Tarizzo P, Stuart F M and Dematteis R 2015 A determination of the molar gas constant R by acoustic thermometry in helium *Metrologia* **52** S274-S304
- [26] Pitre L, Sparasci F, Risegari L, Guianvarc'h C, Martin C, Himbert M E, Plimmer M D, Allard A, Marty B, Giuliano Albo P A, Gao B, Moldover M R and Mehl J B 2017 New measurement of the Boltzmann constant k by acoustic thermometry of helium-4 gas *Metrologia* **54** 856-873
- [27] Feng X J, Zhang J T, Lin H, Gillis K A, Mehl J B, Moldover M R, Zhang K and Duan Y N 2017 Determination of the Boltzmann constant with cylindrical acoustic gas thermometry *Metrologia* **54** 748-762
- [28] de Podesta M, Underwood R, Sutton G, Morantz P, Harris P, Mark D F, Stuart F M, Vargha G and Machin G 2013 A low-uncertainty measurement of the Boltzmann constant *Metrologia* **50** 354–376
- [29] Segovia J J, Lozano-Martín D, Martín M C, Chamorro C R, Villamañán M A, Pérez E, García Izquierdo C and del Campo D 2017 Updated determination of the molar gas constant R by acoustic measurements in argon at UVa-CEM, *Metrologia* **54** 663-673
- [30] Mehl J B 1985 Spherical acoustic resonator: Effects of shell motion *J. Acoust. Soc. Am* **78** 782-788
- [31] Mehl J B 1982 Acoustic resonance frequencies of deformed spherical resonators. *J. Acoust. Soc. Am.* **71** 1109-1113
- [32] Mehl J B 1985 Acoustic resonance frequencies of deformed spherical resonators. II *J. Acoust. Soc. Am.* **78** 278-285
- [33] Pitre L, Sparasci F, Truong D, Guillou A, Risegari L and Himbert M E 2011 Measurement of the Boltzmann constant k_B using a quasi-spherical acoustic resonator *Int. J. Thermophys.* **32** 1825-1886
- [34] Pitre L, Guianvarc'h C, Sparasci F, Guillou A, Truong D, Hermier Y and Himbert M E 2009 An improved acoustic method for the determination of the Boltzmann constant at LNE-INM/CNAM *C. Rendus Physique* **10** 835-848
- [35] Pitre L, Sparasci F, Risegari L, Plimmer M D, Himbert M E and Giuliano Albo P A 2015 Determination of the Boltzmann constant k from the speed of sound in helium gas at the triple point of water *Metrologia* **52** S263-S273
- [36] Zhang J T, Lin H, Feng X J, Sun J P, Gillis K A, Moldover M R and Duan Y Y 2011 Progress toward redetermining the Boltzmann constant with a fixed-path-length cylindrical resonator *Int. J. Thermophys.* **32** 1297-1329
- [37] Lin H, Feng X J, Gillis K A, Moldover M R, Zhang J T, Sun J P and Duan Y Y 2013 Improved determination of the Boltzmann constant using a single, fixed – length cylindrical cavity *Metrologia* **50** 417-432
- [38] Lin H, Gillis K A and Zhang J T 2010 Characterization of piezoelectric ceramic transducer for accurate speed-of-sound measurement *Int. J. Thermophys.* **31** 1234-1247
- [39] Feng X J, Lin H, Gillis K A, Moldover M R and Zhang J T 2015 Test of a virtual cylindrical acoustic resonator for determining the Boltzmann constant *Metrologia* **52** S343-S352
- [40] de Podesta M, May E F, Mehl J B, Pitre L, Gavioso R M, Benedetto G, Giuliano Albo P A, Truong D and Flack D 2010 Characterization of the volume and shape of quasi-spherical resonators using coordinate measurement machines *Metrologia* **47** 588-604

- [41] Underwood R, Davidson S, Perkin M, Morantz P, Sutton G and de Podesta M 2012 Pycnometric volume measurement of a quasispherical resonator *Metrologia* **49** 245-256
- [42] Gillis K A 2012 Second-order boundary corrections to the radial acoustic eigenvalues for a spherical cavity *Metrologia* **49** L21-L24
- [43] de Podesta M, Underwood R, Sutton G, Morantz P, Harris P, Mark D F, Stuart F M and Machin G 2016 Response to Macnaughton's 'Comment on "A low-uncertainty measurement of the Boltzmann constant"' *Metrologia* **53** 116-122
- [44] Yang I, Pitre L, Moldover M R, Zhang J, Feng X and Kim J S 2015 Improving acoustic determinations of the Boltzmann constant with mass spectrometer measurements of the molar mass of argon *Metrologia* **52** S394-S409
- [45] de Podesta M, Yang I, Mark D F, Underwood R, Sutton G and Machin G 2015 Correction of NPL-2013 estimate of the Boltzmann constant for argon isotopic composition and thermal conductivity *Metrologia* **52** S353-S363
- [46] de Podesta M, Mark D F, Dymock R C, Underwood R, Bacquart T, Sutton G, Davidson S and Machin G 2017 Re-estimation of argon isotope ratios leading to a revised estimate of the Boltzmann constant *Metrologia* **54** 683-692
- [47] Pérez-Sanz F J, Segovia J J, Martín M C, Villamañán M A, del Campo D and García C 2015 Progress Towards an Acoustic Determination of the Boltzmann Constant at CEM-UVa *Metrologia* **52** S257-S262
- [48] Gaiser C, Zandt T and Fellmuth B 2015 Dielectric-constant gas thermometry *Metrologia* **52** S217-S226
- [49] Piszczatowski K, Puchalski M, Komasa J, Jeziorski B and Szalewicz K 2015 Frequency-Dependent Polarizability of Helium Including Relativistic Effects with Nuclear Recoil Terms *Phys. Rev. Lett.* **114** 173004
- [50] Zandt T, Fellmuth B, Gaiser C and Kuhn A 2010 Dielectric-Constant Gas-Thermometry Measuring System for the Determination of the Boltzmann Constant at PTB *Int. J. Thermophys.* **31** 1371-1385 and Merlone A, Moro F, Zandt T, Gaiser C and Fellmuth B 2011 Construction and Start-up of a Large-Volume Thermostat for Dielectric-Constant Gas Thermometry *Int. J. Thermophys.* **31** 1386-1395
- [51] Zandt T, Fellmuth B, Gaiser C, Kuhn A, Merlone A, Moro F and Thiele-Krivoi B 2011 Capabilities for Dielectric-Constant Gas Thermometry in a Special Large-Volume Liquid-Bath Thermostat *Int. J. Thermophys.* **32** 1355-1365
- [52] Gaiser C, Fellmuth B, Haft N, Kuhn A, Thiele-Krivoi B, Zandt T, Fischer J, Jusko O and Sabuga W 2017 Final determination of the Boltzmann constant by dielectric-constant gas thermometry *Metrologia* **54** 280-289
- [53] Fellmuth B, Fischer J, Gaiser C, Jusko O, Priruenrom T, Sabuga W and Zandt T 2011 Determination of the Boltzmann constant by dielectric-constant gas thermometry *Metrologia* **48** 382-390
- [54] Maynard J D 1992 The use of piezoelectric film and ultrasound resonance to determine the complete elastic tensor in one measurement *J. Acoust. Soc. Am.* **91** 1754-1762
- [55] Migliori A, Sarrao J L, Visscher W M, Bell T M, Lei M, Fisk Z and Leisure R G 1993 Resonant ultrasound spectroscopic techniques for measurement of the elastic moduli of solids *Physica B* **183** 1-24
- [56] Grüneisen E 1908 Zusammenhang zwischen Kompressibilität, thermischer Ausdehnung, Atomvolumen und Atomwärme der Metalle *Annalen der Physik* **26** 393-402
- [57] Fellmuth B, Bothe H, Haft N, and Melcher J 2011 High-Precision Capacitance Bridge for Dielectric-Constant Gas Thermometry *IEEE Trans. Instr. Meas.* **60** 2522-2526
- [58] Zandt T, Sabuga W, Gaiser C and Fellmuth B 2015 Measurement of pressures up to 7 MPa applying pressure balances for dielectric-constant gas thermometry *Metrologia* **52** S305-S313
- [59] Gaiser C and Fellmuth B 2012 Low-temperature determination of the Boltzmann constant by dielectric-constant gas thermometry *Metrologia* **49** L4-L7
- [60] Gaiser C, Zandt T, Fellmuth B, Fischer J, Jusko O and Sabuga W 2013 Improved determination of the Boltzmann constant by dielectric-constant gas thermometry *Metrologia* **50** L7-L11
- [61] Johnson J B 1927 Thermal Agitation of Electricity in Conductors *Nature* **119** 50-51

- 1
2
3 [62] Johnson J B 1928 Thermal Agitation of Electricity in Conductors *Phys. Rev.* **32** 97-109
- 4 [63] Nyquist H 1928 Thermal Agitation of Electric Charge in Conductors *Phys. Rev.* **32** 110-113
- 5 [64] Callen H B and Welton T A 1951 Irreversibility and Generalized Noise *Phys. Rev.* **83** 34-40
- 6 [65] Brixy H, Hecker R, Oehmen J, Rittinghaus K F, Setiawan W and Zimmermann E 1992 Noise
- 7 thermometry for industrial and metrological applications at KFA Jülich, Schooley J F (Ed.), *Temperature:*
- 8 *Its Measurement and Control in Science and Industry*, vol 6, AIP Proceedings, New York 993-996
- 9 [66] White D R, Galleano R, Actis A, Brixy H, Groot M D, Dubbeldam J, Reesink A L, Edler F, Sakurai H,
- 10 Shepard R L and Gallop J C 1996 The Status of Johnson Noise Thermometry *Metrologia* **33** 325-335
- 11 [67] White D R and Mason R S 2005 An EMI Test for Johnson Noise Thermometry, Zvizdic, Bermanec,
- 12 Veliki and Stasic (Eds.) *Proc. TEMPMEKO 2004, 9th International Symposium on Temperature and*
- 13 *Thermal Measurements in Industry and Science*, Faculty of Mechanical Engineering and Naval
- 14 Architecture, Zagreb 485-490
- 15 [68] Benz S P and Hamilton C A 1996 A pulse-driven programmable Josephson voltage standard *Appl.*
- 16 *Phys. Lett.* **68** 3171-3173
- 17 [69] Benz S P, Hamilton C A, Burroughs C J, Harvey T E, Christian L A and Przybysz J X 1998 Pulse-
- 18 driven Josephson Digital/Analog Converter *IEEE Trans. Appl. Supercond.* **8** 42-47
- 19 [70] Benz S P, Dresselhaus P D, and Martinis J M 2003 An ac Josephson source for Johnson noise
- 20 thermometry *IEEE Trans. Instrum. Meas.* **52** 545-549
- 21 [71] Benz S P, Martinis J M, Nam S W, Tew W L and White D R 2002 A New Approach to Johnson Noise
- 22 Thermometry using a Josephson Quantized Voltage Source for Calibration, Fellmuth B., Seidel J., Scholz
- 23 G. (Eds.), *Proc. TEMPMEKO 2001, 8th International Symposium on Temperature and Thermal*
- 24 *Measurements in Industry and Science*, VDE Verlag, Berlin 37-44
- 25 [72] Nam S W, Benz S P, Dresselhaus P D, Tew W L, White D R and Martinis J M 2003 Johnson noise
- 26 thermometry measurements using a quantum voltage noise source for calibration, *IEEE Trans. Instrum.*
- 27 *Meas.* **52** 550-553
- 28 [73] Benz S P, White D R, Qu J, Rogalla H and Tew W L 2009 Electronic measurement of the Boltzmann
- 29 constant with a quantum-voltage-calibrated Johnson-noise thermometer *C. Rendus Physique* **10** 849-858
- 30 [74] White D R and Benz S P 2008 Constraints on a Synthetic-Noise Source for Johnson Noise
- 31 Thermometry *Metrologia* **45** 93-101
- 32 [75] White D R, Benz S P, Labenski J R, Nam S W, Qu J F, Rogalla H and Tew W L 2008 Measurement
- 33 time and statistics for a noise thermometer with a synthetic-noise reference *Metrologia* **45** 395-405
- 34 [76] Qu J F, Benz S P, Rogalla H and White D R 2009 Reduced nonlinearities and improved temperature
- 35 measurements for the NIST Johnson noise thermometer *Metrologia* **46** 512-524
- 36 [77] Benz S P, Pollarolo A, Qu J F, Rogalla H, Urano C, Tew W L, Dresselhaus P D and White D R 2011
- 37 An electronic measurement of the Boltzmann constant *Metrologia* **48** 142-153
- 38 [78] Qu J F, Benz S P, Pollarolo A, Rogalla H 2011 Reduced nonlinearity effect on the electronic
- 39 measurement of the Boltzmann constant *IEEE Trans. Instrum. Meas.* **60** 2427-2433
- 40 [79] Pollarolo A, Jeong T, Benz S P and Rogalla H 2013 Johnson Noise Thermometry Measurement of
- 41 the Boltzmann Constant With a 200 Ω Sense Resistor *IEEE Trans. Instrum. Meas.* **62** 1512-1517
- 42 [80] Qu J F, Fu Y F, Zhang J Q, Rogalla H, Pollarolo A and Benz S P 2013 Flat frequency response in the
- 43 electronic measurement of the Boltzmann constant measurement *IEEE Trans. Instrum. Meas.* **62** 1518-
- 44 1523
- 45 [81] Qu J F, Zhang J T, Fu Y F, Rogalla H, Pollarolo A, and Benz S P 2013 Development of a quantum-
- 46 voltage-calibrated noise thermometer at NIM, C W Meyer (Ed.) *Temperature: Its Measurement and*
- 47 *Control in Science and Industry*, vol 8, AIP Proceedings, New York **1552** 29-33
- 48 [82] Qu J F, Benz S P, Pollarolo A, Rogalla H, Tew W L, White R D, and Zhou K L 2015 Improved
- 49 electronic measurement of the Boltzmann constant by Johnson noise Thermometry *Metrologia* **52** S242-
- 50 S256
- 51 [83] White R D and Qu J F 2017 Frequency-response mismatch effects in Johnson noise thermometry
- 52 *Metrologia* **54** accepted, doi.org/10.1088/1681-7575/aa963c
- 53
54
55
56
57
58
59
60

- 1
2
3 [84] Coakley K J and Qu J F 2017 Spectral model selection in the electronic measurement of the
4 Boltzmann constant by Johnson noise thermometry *Metrologia* **54** 204-217
- 5 [85] Qu J F, Benz S P, Coakley K J, Rogalla H, Tew W L, White R D, Zhou K L and Zhou Z Y 2017 An
6 improved electronic determination of the Boltzmann constant by Johnson noise thermometry *Metrologia*
7 **54** 549-558
- 8 [86] Mills I M, Mohr P J, Quinn T J, Taylor B N and Williams E R 2006 Redefinition of the kilogram,
9 ampere, kelvin and mole: a proposed approach to implementing CIPM recommendation 1 (CI-2005)
10 *Metrologia* **43** 227-246
- 11 [87] Flowers-Jacobs N E, Pollarolo A, Coakley K J, Fox A E, Rogalla H, Tew W L and Benz S P 2017 A
12 Boltzmann constant determination based on Johnson noise thermometry *Metrologia* **54** 730-737
- 13 [88] Urano C, Yamazawa K and Kaneko N-H 2017 Measurement of the Boltzmann constant by Johnson
14 noise thermometry using superconducting integrated circuit *Metrologia* **54** 847-855
- 15 [89] Bordé C J 2002 Atomic clocks and inertial sensors *Metrologia* **39** 435-463
- 16 [90] Daussy C, Guinet M, Amy-Klein A, Djerroud K, Hermier Y, Briaudeau S, Bordé C J and Chardonnet
17 C 2007 Direct Determination of the Boltzmann Constant by an Optical Method *Phys. Rev. Lett.* **98** 250801
- 18 [91] Lemarchand C, Triki M, Darquie B, Borde C J, Chardonnet C and Daussy C 2011 Progress towards
19 an accurate determination of the Boltzmann constant by Doppler spectroscopy *New Journal of Physics* **13**
20 073028
- 21 [92] Bernard V, Daussy C, Nogues G, Constantin L, Durand P E, Amy-Klein A, van Lerberghe A and
22 Chardonnet C 1997 CO₂ laser stabilization to 0.1-Hz level using external electrooptic modulation *IEEE*
23 *Journal of Quantum Electronics* **QE-33** 1282-1287
- 24 [93] Lemarchand C, Djerroud K, Darquie B, Lopez O, Amy-Klein A, Chardonnet C, Bordé C J, Briaudeau
25 S and Daussy C 2010 Determination of the Boltzmann Constant by Laser Spectroscopy as a Basis for
26 Future Measurements of the Thermodynamic Temperature *Int. J. Thermophys.* **31** 1347-1359
- 27 [94] Lemarchand C, Mejri S, Sow P L T, Triki M, Tokunaga S K, Briaudeau S, Chardonnet C, Darquie B
28 and Daussy C 2013 A revised uncertainty budget for measuring the Boltzmann constant using the
29 Doppler broadening technique on ammonia *Metrologia* **50** 623-630
- 30 [95] Triki M, Lemarchand C, Darquie B, Sow P L T, Roncin V, Chardonnet C and Daussy C 2012 Speed-
31 dependent effects in NH₃ self-broadened spectra: Towards the determination of the Boltzmann constant
32 *Phys. Rev. A* **85** 062510
- 33 [96] Rohart F, Mejri S, Sow L and Daussy C 2014 Absorption-line-shape recovery beyond the detection-
34 bandwidth limit: Application to the precision spectroscopic measurement of the Boltzmann constant *Phys.*
35 *Rev. A* **90** 042506
- 36 [97] Mejri S, Sow P L T, Kozlova O, Ayari C, Tokunaga S K, Chardonnet C, Briaudeau S, Darquie B,
37 Rohart F and Daussy C 2015 Measuring the Boltzmann constant by mid-infrared laser spectroscopy of
38 ammonia *Metrologia* **52** S314-S323
- 39 [98] Sow P L T, Mejri S, Tokunaga S K, Lopez O, Goncharov A, Argence B, Chardonnet C, Amy-Klein A,
40 Daussy C and Darquie B 2014 A widely tunable 10 μm quantum cascade laser phase-locked to a state-
41 of-the-art mid-infrared reference for precision molecular spectroscopy *Appl. Phys. Lett.* **104** 264101
- 42 [99] Gianfrani L 2016 Linking the thermodynamic temperature to an optical frequency: recent advances in
43 Doppler broadening thermometry *Phil. Trans. R. Soc. A* **374** 20150047
- 44 [100] Casa G, Castrillo A, Galzerano G, Wehr R, Merlone A, Di Serafino D, Laporta P and Gianfrani L
45 2008 Primary gas thermometry by means of laser-absorption spectroscopy: determination of the
46 Boltzmann constant *Phys. Rev. Lett.* **100** 200801
- 47 [101] Moretti L, Castrillo A, Fasci E, De Vizia M D, Casa G, Galzerano G, Merlone A, Laporta P and
48 Gianfrani L 2013 Determination of the Boltzmann constant by means of precision measurements of H₂¹⁸O
49 line shapes at 1.39 μm *Phys. Rev. Lett.* **111** 060803
- 50 [102] Castrillo A, Moretti L, Fasci E, De Vizia M D, Casa G and Gianfrani L 2014 The Boltzmann constant
51 from the shape of a molecular spectral line *J. Mol. Spectrosc.* **300** 131-138
- 52
53
54
55
56
57
58
59
60

- 1
2
3 [103] Fasci E, De Vizia M D, Merlone A, Moretti L, Castrillo A and Gianfrani L 2015 The Boltzmann
4 constant from the H₂¹⁸O vibration-rotation spectrum: complementary tests and revised uncertainty budget
5 *Metrologia* **52** S233–S241
- 6 [104] De Vizia M D, Odintsova T and Gianfrani L 2016 Hyperfine structure effects in Doppler-broadening
7 thermometry on water vapor at 1.4 μm *Metrologia* **53** 800–804
- 8
9 [105] Castrillo A, De Vizia M D, Fasci E, Odintsova E, Moretti L and Gianfrani L 2016 Doppler-Broadening
10 Gas Thermometry at 1.39 μm: Towards a New Spectroscopic Determination of the Boltzmann Constant,
11 K Dieckmann (Ed.) *Laser Spectroscopy - Proceedings of the XXII International Conference World*
12 *Scientific Publishing, Singapore* 31-41
- 13 [106] Fasci E, Odintsova T, Castrillo A, De Vizia M D, Merlone A, Bertiglia F, Moretti L and Gianfrani L
14 2016 Dual-laser absorption spectroscopy of C₂H₂ at 1.4 μm *Phys. Rev. A* **93**, 042513
- 15 [107] Amodio P, De Vizia M D, Moretti L and Gianfrani L 2015 Investigating the ultimate accuracy of
16 Doppler-broadening thermometry by means of a global fitting procedure *Phys. Rev. A* **92** 032506
- 17 [108] Preston-Thomas H 1990 The International Temperature Scale of 1990 (ITS-90) *Metrologia* **27** 3-10;
18 www.bipm.org/en/publications/its-90.html
- 19 [109] The International Systems of Units, 9th Brochure, BIPM Cons. Com. Units 2017;
20 www.bipm.org/en/committees/cc/ccu/publications-cc.html
- 21
22 [110] Anhalt K, Machin G 2016 Thermodynamic temperature by primary radiometry *Phil. Trans. R. Soc. A*
23 **374** 20150041
- 24 [111] Sutton G, Underwood R, Pitre L, de Podesta M and Valkiers S 2010 Acoustic Resonator
25 Experiments at the Triple Point of Water: First Results for the Boltzmann Constant and Remaining
26 Challenges *Int. J. Thermophys.* **31** 1310-1346
- 27 [112] Gavioso R M, Benedetto G, Giuliano Albo P A, Madonna Ripa D, Merlone A, Guianvarc'h C, Moro F
28 and Cuccaro R 2010 A determination of the Boltzmann constant from speed of sound measurements in
29 helium at a single thermodynamic state *Metrologia* **47** 387-409
- 30 [113] Moldover M R, Gavioso R M and Newell D B 2015 Correlations among acoustic measurements of
31 the Boltzmann constant *Metrologia* **52** S376–S384
- 32
33
34
35
36
37
38
39
40
41
42
43
44
45
46
47
48
49
50
51
52
53
54
55
56
57
58
59
60